

Online Research @ Cardiff

This is an Open Access document downloaded from ORCA, Cardiff University's institutional repository: <https://orca.cardiff.ac.uk/id/eprint/125519/>

This is the author's version of a work that was submitted to / accepted for publication.

Citation for final published version:

Yang, Alexandra Yang, Wang, Chunguang, Liang, Yan and Lissenberg, C. Johan
ORCID: <https://orcid.org/0000-0001-7774-2297> 2019. Reaction between mid-ocean ridge basalt and lower oceanic crust: an experimental study. *Geochemistry, Geophysics, Geosystems* 20 (9) , 4390 - 4407.
10.1029/2019GC008368 file

Publishers page: <http://dx.doi.org/10.1029/2019GC008368>
<<http://dx.doi.org/10.1029/2019GC008368>>

Please note:

Changes made as a result of publishing processes such as copy-editing, formatting and page numbers may not be reflected in this version. For the definitive version of this publication, please refer to the published source. You are advised to consult the publisher's version if you wish to cite this paper.

This version is being made available in accordance with publisher policies.

See

<http://orca.cf.ac.uk/policies.html> for usage policies. Copyright and moral rights for publications made available in ORCA are retained by the copyright holders.



Reaction between mid-ocean ridge basalt and lower oceanic crust: An experimental study

Alexandra Yang Yang^{1,2}, Chunguang Wang³, Yan Liang⁴, C. Johan Lissenberg²

¹Key laboratory of Ocean and Marginal Sea Geology, Guangzhou Institute of Geochemistry, Chinese Academy of Sciences, Guangzhou, 510640, China.

²School of Earth and Ocean Sciences, Cardiff University, Park Place, Cardiff CF10 3AT, UK.

³College of Earth Sciences, Jilin University, Changchun 130061, China.

⁴Department of Geological Sciences, Brown University, Providence, RI 02912, USA

Corresponding author: Alexandra Yang Yang (yangyang@gig.ac.cn)

Key Points:

- Melt-mush reactions proceed through diffusion-assisted dissolution and reprecipitation.
- Reaction significantly shifts melt major element compositions, indicating it can limit the application of major-element barometers for MORB.
- Clinopyroxene Mg#-Na-Ti and olivine Fo-Ni relationships in cumulates provide tracers for melt-mush reaction in nature.

Abstract

Reaction between mid-ocean ridge basalt (MORB) and crystal mush in the lower oceanic crust has been invoked to explain chemical variations of both MORB and minerals in the lower oceanic crust. Nonetheless, such reactions have been little studied experimentally. We conducted experiments to investigate the mechanisms and chemical consequences of melt-mush interaction by reacting molten MORB with troctolite at 0.5 GPa. Isothermal experiments demonstrate that melt infiltrates into troctolite with dissolution of plagioclase and olivine. The reacted melts have higher MgO and Al₂O₃ and lower TiO₂ and Na₂O contents, and crystallize more primitive olivine and plagioclase compared to those crystallized from the unreacted melts, suggesting melt-mush reaction could result in the formation of high-Al basalt. The melt composition variations induced by reaction also significantly affects the calculated pressures for MORB fractionation, indicating that major element-based barometers for MORB fractionation can only be used reliably if reaction can be ruled out. After reaction, the troctolite contains olivine with plagioclase inclusions and poikilitic clinopyroxene with partially resorbed olivine and plagioclase chadacrysts, indicating that melt-mush interaction occurs through dissolution-reprecipitation mechanisms. Clinopyroxene has high Mg# (>83) and elevated Na₂O and TiO₂ contents, and olivine has different Fo vs. Ni correlations from fractional crystallization models, which provide testable parameters for the effect of melt-mush reaction in the rock record. By comparison with samples from lower oceanic crust and layered intrusions, we propose that melt-mush reaction plays an important role during magma transport in the crystal mush in both oceanic and continental magma systems.

Plain Language Summary

Magmas erupted at mid-ocean ridges represent the largest volcanic output from the Earth's interior, and have long been recognized as a probe to mantle composition and melting history. During its ascent from the mantle, magma crystallizes minerals in crustal magma reservoirs. Although crystallization modifies magma compositions, this process is well-understood and can therefore be corrected for. However, when crystallization proceeds, a network of interconnected minerals forms with small amounts of magma between them. Recent studies show that magma compositions might also be modified by reaction with minerals in this so-called crystal mush. Our study, for the first time, performed experiments to explore how such reactions work, and how they change the compositions of both magma and minerals. The results show that during reaction, magma can dissolve some minerals and crystallize others, which changes the magma compositions. Such variations in magma compositions challenge our understanding on the histories, depth of magma crystallization derived from them, and eventually affect our understanding of mantle composition. We also found that minerals in the mush carry distinct chemical signatures after reaction, which can be used as tracers for melt-mush reaction in nature. Comparison with natural mineral data suggests that such reaction is common in magma systems.

1 Introduction

Mid-ocean ridge basalt (MORB) has long been recognized as a probe to the composition of the upper mantle. Crustal level modifications to MORB compositions are largely attributed to fractional crystallization, which can be corrected through parameterizations of experimental data or thermodynamic calculations (e.g., Grove et al., 1992; Langmuir et al., 1992). However, studies on both MORB and plutonic rocks from the lower oceanic crust have provided evidence suggesting that the crustal evolution of MORB is complex, involving more than fractional crystallization alone (e.g., Lissenberg & MacLeod, 2016 and reference therein). Seismic studies indicate that mid-ocean ridges are mostly underlain by crystal mush (Canales et al., 2000; Carbotte et al., 2013; Crawford & Webb, 2002; Crawford et al., 1999; Dunn et al., 2000; Seher et al., 2010; Vera et al., 1990). Hence, melts and crystals coexist throughout the mid-ocean ridge magma plumbing system, providing two possible mechanisms for reactions to occur between melts and crystals. The first is during the emplacement of primitive melts into the mush (Kvassnes & Grove, 2008; Leuthold et al., 2018). Primitive melts are unlikely to be saturated in (all of) the phases present in the mush in which they are emplaced, leading to partial melting reactions. The second is during upward flow of interstitial melts in the mush (Coogan et al., 2000a; Gao et al., 2007; Lissenberg & Dick, 2008; Lissenberg et al., 2013). Numerical modeling of this process indicates that melt migrating through such a compacting mush will react with the constituent crystals (Solano et al., 2014), which is consistent with the rock record (Lissenberg & MacLeod, 2016). Therefore, melt-mush reaction is a natural consequence of the emplacement of primitive melt into the lower oceanic crust, and the percolation of (evolved) interstitial melt through the crystal mush.

Lower oceanic crustal sections exposed and/or drilled have provided a wealth of observations on the role of reactions in the magmatic evolution of the lower oceanic crust. This includes: Hess Deep in the East Pacific Rise (Coogan et al., 2002; Lissenberg et al., 2013); the Kane area (Coogan et al., 2000; Dick et al., 2008; Lissenberg & Dick, 2008), Atlantis Massif (Blackman et al., 2011), and 16.5°N (Sanfilippo et al., 2019) along the Mid-Atlantic Ridge; Atlantis Bank along the Southwest Indian Ridge (Dick et al., 2000; Gao et al., 2007; Lissenberg & MacLeod, 2016); Uraniwa Hills from the Central Indian Ridge (Sanfilippo et al., 2015a); and Godzilla Megamullion in the Parece Vela back-arc basin (Sanfilippo et al., 2013). Further evidence is present in the plutonic sections of ophiolites (Basch et al., 2018, 2019; Bédard, 1991; Bedard et al., 2000; Rampone et al., 2016; Sanfilippo et al., 2015b). The samples revealed complex zoning patterns, reaction textures, as well as mineral compositions and modes that could not be explained by fractional crystallization: instead, the data suggest that melt-mush reaction is a common process in the lower oceanic crust (Coogan et al., 2000a; Dick et al., 2002; Gao et al., 2007; Leuthold et al., 2018; Lissenberg & MacLeod, 2016; Lissenberg et al., 2013; Meyer et al., 1989; Ridley et al., 2006). Such a melt-mush reaction is also proposed to be common in continental magma systems (e.g., Bédard et al., 1988; Boudreau, 1999; Cashman et al., 2017; Irvine, 1980; Leuthold et al., 2015; Leuthold et al., 2014; Mathez, 1995; McBirney & Sonnenthal, 1990; Namur et al., 2013).

Phenocrysts and xenoliths in MORB samples provide further evidence of magma replenishment and subsequent reaction. Glassy MORB samples are widely known to host olivine and plagioclase crystals which are commonly not in equilibrium with their surrounding glass (Moore et al., 2014; Pan & Batiza, 2002, 2003; Bennett et al., 2019). Some of these samples contain phenocrysts proportions as high as 50% (Hellevang & Pedersen, 2008; Lange et al., 2013; Bennett et al., 2019), suggesting physical mixing and/or chemical reaction between a phenocryst-poor magma with a crystal-bearing mush. Melt-bearing cumulate xenoliths in MORB from the East

Pacific Rise and Iceland provide strong evidence for complex melt-mush reaction history in the lower oceanic crust, including the passage of multiple MORB magmas through the network of intergranular pores, and disequilibrium-induced dissolution and subsequent growth of crystals in the mush (Gurenko & Sobolev, 2006; Ridley et al., 2006). High-Al melt inclusion in olivine in MORB (e.g., Danyushevsky et al., 2003; Koleszar et al., 2009; Laubier et al., 2012) and high-Al MORB (e.g., Coumans et al., 2016; Yang et al., 2017), mostly with high MgO (>8 wt.%), were all proposed to form by reaction with a plagioclase-bearing cumulate in the lower oceanic crust.

Hence, the available data indicate that disequilibrium induced by both replenishment and porous flow of melt through a crystal mush is common in the magma plumbing system, and that the resulting reactions may play an important role in the evolution of the oceanic crust. Experimental works have been devoted to the reaction of melt with mantle rocks, including peridotite (e.g., Daines & Kohlstedt, 1994; Lambart et al., 2009; Morgan & Liang, 2003, 2005; Saper & Liang, 2014; Tursack & Liang, 2012; Van Den Bleeken et al., 2010, 2011; Wang et al., 2013), and dunite (e.g., Borghini et al., 2018), but very little attention has been paid to reaction of melt with crustal cumulates. Melt-cumulate interaction experiments have been conducted by melting plagioclase-olivine and plagioclase-augite mineral pairs at temperatures much higher than the melt-mineral saturation boundary (Kvassnes & Grove, 2008), which could be applicable during emplacement of primitive melt in a mush. However, in natural conditions, such interaction might not simply occur by melting cumulates and subsequent mixing with preexisting melt, especially during flow of interstitial melts in a primitive cumulate framework. Thus, it remains poorly understood by which mechanisms melt-mush reactions proceed, how and to what extent such processes would change MORB compositions and hence, how such interaction will affect reconstructions of mantle source compositions and melting processes. We conducted a series of melt-mush reaction experiments to investigate the mechanism and chemical consequences of such process by reacting both primitive and evolved MORB melts with a primitive cumulate (troctolite). The results have enabled a reconstruction of the melt-mush reaction mechanisms, and place constraints on the chemical consequences of melt-mush reaction on both the plutonic rocks and the melt.

2 Experimental methods

Reactive crystallization experiments characterizing melt-mush interaction were conducted at 1180°C and 1200°C (corresponding to the estimated liquidus temperatures for the two starting melts) and 0.5 GPa for 6-27 hrs using a 19.1-mm piston cylinder apparatus at Brown University. The reaction couple was formed by juxtaposing a powdered MORB against a troctolite in a graphite-lined molybdenum capsule (Figure 1).

2.1 Starting materials

The starting materials for the melts are a powdered primitive MORB glass with Mg# (defined as mole fractions of $100 \times \text{MgO}/(\text{MgO} + \text{FeO}^{\text{T}})$) of 64 (KN182-13 D44A, provided by Alberto Saal) and moderately evolved MORB from the East Pacific Rise (Mg# 54; MOA8712-095, provided by John Sinton), with the latter representing average East Pacific Rise basalts. A lower oceanic crust troctolite analog was produced by combining 70 wt.% unzoned plagioclase (anorthite (An) 87, from Oman ophiolite gabbro sample 97OB1, provided by Benoit Ildefonse) and 30 wt.% unzoned olivine (forsterite (Fo) 90, from Kilbourne Hole, New Mexico, Sample KBH-1). In addition, a troctolitic mush analog was produced by combining 45 wt.% plagioclase, 45 wt.% olivine and 10% interstitial primitive MORB glass of the same origin. Optically clean

mineral grains of approximately 100-150 μm and glass chips of around 1-3 mm were first hand separated under a binocular microscope, mixed based on the appropriate weight percentages, and then ground under ethanol to obtain the desired starting materials. Afterward, the basalts and troctolite were stored in closed containers in a 110°C oven. Table 1 lists the starting mineral and melt compositions.

2.2 Experimental procedure

The experimental procedure was similar to that described in Tursack and Liang (2012) and Saper and Liang (2014). The furnace assembly consists of a molybdenum capsule in an MgO sleeve sandwiched between two crushable MgO spacers in a graphite, Pyrex and KCl salt sleeve. The molybdenum capsule (6.5 mm outer diameter and 10 mm long) was lined with a graphite inner sleeve (4 mm outer diameter, 2 mm inner diameter), which served as an inert buffer between molybdenum and the silicates. To form a reaction couple, we packed the bottom 2-3 mm of the graphite inner capsule with troctolite and the top 3-4 mm with the powdered basalt. The top of the capsule was then sealed with a 1-mm layer of graphite powder, and capped with a molybdenum lid (0.5-1 mm thick) (Figure 1). The furnace assembly was held in a 110°C oven for at least 12 hrs.

The furnace assembly was wrapped with lead foil and loaded into the piston cylinder apparatus. To run an experiment, the assembly was first cold pressurized to slightly above 0.5 GPa. The temperature was then ramped to 1180°C (evolved melt) or 1200°C (primitive melt) at a rate of 75°C/min. After 6 hrs (27 hrs for run TE_Ls) of reaction at the target temperatures, runs TE1, TE_mush and TP1 were quenched, and the others were step-cooled to 1000°C (evolved melt) or 1050°C (primitive melt) and subsequently quenched following the temperature-time history displayed in Figure 1. Pressure was kept at 0.5 GPa throughout the experiment. Temperature was measured using a W₉₇Re₃-W₇₅Re₂₅ thermocouple and monitored using a Eurotherm controller with an uncertainty of 10°C (Morgan & Liang, 2005). After quenching the experiment, the charge was unloaded and the molybdenum capsule was extracted and sectioned longitudinally. The sectioned charges were mounted in epoxy, polished, and carbon coated for electron microprobe (EMPA) and scanning electron microscope (SEM) analyses (detailed methods can be found in the Supporting Information).

3 Results

Eight melt-mush reaction experiments were conducted in this study, supplemented by two runs on the melts alone. Figure 1 and Table 2 summarize the temperature-time history of the ten runs. Five experiments used the troctolite (T, 70% plagioclase, 30% olivine) and evolved MORB (E) melt (runs TE1, TE2, TE_FC, TE_SC, and TE_Ls) and two the troctolite and primitive MORB (P; runs TP1 and TP2). The other melt-mush reaction experiment used evolved MORB and the troctolitic mush (45% olivine, 45% plagioclase and 10% primitive MORB; run TE_mush).

Because we used the liquidus temperatures of the melts during the experiments, the basalt was liquid and troctolite was mainly solid with varied proportions of interstitial melt. In addition, two step-cooling experiments with the evolved and primitive MORB melts only (i.e., without troctolite; runs Es and Ps) were conducted as a reference to compare the crystallization sequence with and without reaction at the same pressure. Except for TE_Ls, all runs were reacted at the respective liquidus temperatures for 6 h. TE1, TP1 and TE_mush were quenched directly after 6 h reaction. TE2/Es and TP2/Ps were step-cooled to 1000°C and 1050°C, respectively. TE_FC and

TE_SC were cooled with constant cooling rates at 1°C/min and 0.1°C/min, respectively, to compare whether varied cooling rates would affect the results of the reaction experiment. TE_Ls is a long duration run, which was reacted at 1180°C for 27 h before step-cooling to 1000°C. Our reaction experiments produced a variety of reaction textures and mineral compositional variations depending on the run conditions and the compositions of the reacting melt.

3.1 Textures of reactive products

3.1.1 Isothermal experiments: Melt infiltration into the troctolite with dissolution of olivine and plagioclase

Isothermal experiments TE_mush, TE1, and TP1 all produced basalt at the top and interstitial melt-bearing troctolite at the bottom (Figure 2 and Figure S1 in Supporting Information). Euhedral clinopyroxenes crystallized in the upper part of the melt in TE1 (Figure S1a in Supporting Information). Relatively large olivines (~100 µm in length) crystallized near the melt-troctolite interface, and small olivine and plagioclase crystals are present in the upper part of the melt in run TP1 (Figure S1b in Supporting Information).

Interstitial melt phase in both TE1 and TP1 runs are volumetrically less than those in TE_mush run due to the absence of melt phase in the starting troctolite in the former two runs (Figure S1 in Supporting Information). Nonetheless, melt infiltrated the troctolite in TE1 and TP1, with the amount of the interstitial melt gradually decreasing away from the melt-troctolite interface, forming a melt infiltration zone in the upper part of the troctolite (Figure 2). Plagioclase grains, much smaller than the starting plagioclase and mostly round in shape, were found to be included in olivine grains in the melt infiltration zone (Figure 2b). These plagioclase-bearing olivines are euhedral, in contrast to olivine grains below the zone. Because no plagioclase inclusions were present in the olivine starting material, this observation indicates that the euhedral olivine was precipitated either during or after plagioclase was partially dissolved.

3.1.2 Step-cooling experiments: clinopyroxene precipitated as reaction product

Step-cooling experiments produced olivine-bearing gabbro and clinopyroxene-bearing troctolite from top to bottom (Figure 3). In the long duration run TE_Ls, the gabbros contain relatively large clinopyroxene grains, feldspar laths, olivine, sulfide, and melt. Interstitial melt and clinopyroxene were present throughout the troctolite (Figure 3). Clinopyroxene shows poikilitic textures with olivine and plagioclase chadacrysts (Figure 3d), forming darker patches in the troctolite relative to interstitial melt bearing troctolite with a lighter green color in the element map (Figure 3a).

3.2 Chemical consequences of melt-mush reaction

3.2.1 Chemical variations of melts in isothermal experiments

Overall, melt compositions gradually shift to higher MgO and Al₂O₃, lower FeO, and slightly lower TiO₂, and Na₂O contents towards the melt-troctolite interface (Figure 4). Mg# in the melt increased progressively from the original values for evolved and primitive melts at 54 and 64, to the highest values close to the melt-troctolite interface at 59 and 68 for runs TE1 and TP1, respectively (Figure 4). Mg# of the melt at the interface of run TE_mush increased to 68 at the interface, and further up to 74 for the interstitial melt in the troctolite (Figure 4). Due to the

crystallization of clinopyroxene in the upper part of the melt in run TE1, where the temperature is slightly lower than the center of the capsule (due to presence of a temperature gradient), melt compositions here shifted to higher Al_2O_3 , lower MgO and FeO contents (Figure 4).

The large olivine crystals in the melt close to the melt-troctolite interface in run TP1 (Figure S1b in Supporting Information) have similar compositions (Fo 87.3) to those in the troctolite near the interface (Fo 87.5). Melts and olivine in the troctolite near interface in runs TE1, TE_mush and TP1 as well as interstitial melt and olivine in the troctolite in TE_mush all show Mg-Fe equilibrium (Figure 5). These observations suggests equilibrium of melt and troctolite near the interface.

3.2.2 Shifts in melt fractionation sequences following reaction: step-cooling experiments

To compare the melt fractionation sequence before and after reaction, step-cooling experiments of the two starting melts (i.e., without troctolite) were run. The highest Mg# of clinopyroxene and Fo of olivine in the melt phase in the step-cooling experiments can be used to discriminate whether clinopyroxene or olivine is the first phase to crystallize in the melt (Figure 6). If the two are in Mg-Fe equilibrium, the melt should be close to olivine and clinopyroxene cotectic at the onset of crystallization. If the former plots above the equilibrium field (Figure 6), clinopyroxene is likely to have crystallized earlier than olivine, and vice versa. The mineral compositions in the step-cooling experiment for evolved melt only (run Es) are clinopyroxene with Mg# up to 82, and plagioclase with An up to 59 (not in Figure 6 due to the absence of olivine in run Es). After 6 h reaction with troctolite in TE1, melt compositions at the melt-troctolite interface have higher MgO, and Al_2O_3 contents. In the corresponding step-cooling experiments TE2, TE_FC, TE_SC and TE_Ls, clinopyroxene (Mg# up to 83-86) and olivine (Fo up to 80-85) in the gabbro sections are roughly in Mg-Fe equilibrium (Figure 6) and are thus close to cotectic. Plagioclase in these runs also have much higher An than those in run Es (up to 66-76, +17 mol%). Therefore, reaction with a primitive troctolite caused the melt, which was originally saturated with clinopyroxene as ferromagnesian phase, to be co-saturated with olivine. Furthermore, reaction led the melt to crystallize more primitive olivine, clinopyroxene and plagioclase during magma evolution than it would have done without reaction.

The mineral compositions in the step-cooling experiment for primitive melt only (run Ps) are olivine with Fo up to 84, clinopyroxene with Mg# up to 87, and plagioclase with An up to 68, with clinopyroxene and olivine in Mg-Fe equilibrium, indicating that magma evolution of the primitive melt at the run pressure should start with cotectic olivine and clinopyroxene followed by plagioclase fractionation. After 6 h reaction with troctolite in TP1, melt compositions at the melt-troctolite interface have higher MgO, and Al_2O_3 contents. In the corresponding step-cooling run TP2, spinel crystals are found at the interface, and the reacted melt crystallized more primitive olivine (Fo up to 87, +3 mol%) and plagioclase (An up to 77, +9 mol%), and less primitive clinopyroxene (Mg# up to 82, -5 mol%) compared to run Ps (Figure 6). The presence of olivine crystals in melt phase near the melt-troctolite interface of run TP1 also indicates that olivine was the first phase to crystallize after reaction.

Although plagioclase crystallization is likely suppressed by the slightly higher pressure of 0.5 GPa of the experiment compared to typical lower oceanic crustal conditions (0.1-0.2 GPa), the findings of more primitive olivine and plagioclase compositions after reaction with a primitive troctolite should apply at lower pressures as well. Clinopyroxene crystallized from the reacted melt, on the other hand, increased in Mg# from 82 to up to 86 in TE runs, but decreased from 87 in run Ps to 82 in run TP2. Extensive olivine crystallization in the melt in run TP2 may have

lowered the melt in MgO contents, which thereafter crystallized clinopyroxene with lower Mg# than run Ps.

3.2.3 Troctolite compositional variations

The starting olivine in the troctolite has Fo of ~90 and NiO contents of ~0.37 wt.%. After reaction, the olivine compositions show a general decrease in both Fo and NiO contents towards the melt-troctolite interface in all runs (Figure 7a, b). Variations of olivine compositions in the troctolite are controlled by both the starting melt compositions and run durations. In isothermal experiments of TP1 and TE1 with same duration (6 h), olivine cores show significant shifts in the first 400 μm of the troctolite (Figure 7a, b), corresponding to ~400 μm melt infiltration (Figure 2 and Figure S1 in Supporting Information). The far-field olivine in the troctolite retains same compositions to the starting olivine within error, and were hence not affected significantly by reactive melt infiltration. In contrast, the olivine core compositions in the troctolite of long-duration run TE_Ls are characterized by more evolved compositions through the entire troctolite section, and are spatially more homogeneous, indicating that melt infiltrated and reacted to the end of the troctolite.

Olivines show sharper decreases in Fo for TE1 than TP1, as would be predicted by the differences in melt composition: melt Mg#-olivine Fo relationships (Figure 5) suggest that chemical equilibrium has been achieved at the interface of both TE and TP runs after 6 h reaction, indicating Fo in olivine are controlled by the Mg-Fe equilibrium between melt and troctolite. Hence, lower Mg# of the evolved melt leads to lower Fo in the olivines after reaction. In contrast to Fo, Ni in olivine compositions are similar between TP1 and TE1 (Figure 7a). Plagioclase, on the other hand, show clear core-to-rim variations with cores in all runs retaining their original compositions and rims having lower An numbers towards the melt-troctolite interface (Figure 7c). Interstitial clinopyroxene in the reacted troctolite in the step-cooling runs have high Na₂O and TiO₂ contents (up to 0.81, and 2.51 wt.%, respectively) with high Mg# (>83).

4 Discussion

Melt and mineral compositions vary systematically across experimental charges. Through reaction with troctolite, melts become more enriched in MgO and Al₂O₃ and depleted in TiO₂ and Na₂O contents, and crystallize more primitive olivine and plagioclase compared to those crystallized from the starting melts. On the other hand, the troctolite shifted to more evolved compositions to be equilibrated with the melt near the melt-troctolite interface. These chemical variations record the progression of melt-mush reaction and provide important clues to the mechanisms of melt-mush interaction.

4.1 Mechanism of melt-mush reaction: diffusion-assisted dissolution and reprecipitation

Collectively, the observation of interstitial melt in the troctolite in runs TE1 and TP1, the gradual decrease in melt fraction further into the troctolite, and plagioclase relicts in euhedral olivines (Figure 2), suggest the incipient melt infiltration into the troctolite and the dissolution of plagioclase + olivine by melt. Plagioclase relicts in olivines can be explained by different dissolution and reprecipitation rates of olivine and plagioclase. Experimental study of the dissolution of olivine and plagioclase in basaltic magma suggest dissolution of plagioclase is ~6 times faster than olivine, whereas the growth rate of plagioclase is at least 10 times slower than olivine (Donaldson, 1985). Hence, it is likely that melt dissolved plagioclase rapidly with minor

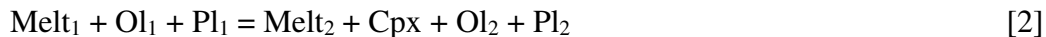
plagioclase reprecipitation, whereas olivine was more likely to be dissolved and reprecipitated simultaneously. Therefore, during dissolution and precipitation of olivine, plagioclase is partially dissolved and the relic grains were incorporated into growing olivine crystals (euhedral in Figure 2b).

The chemical variations of olivine and plagioclase in the troctolite after reaction show different characteristics, also suggesting different reaction mechanism for olivine and plagioclase. Even the core compositions of olivine crystals have been modified in all the experiments. In contrast to olivine, the cores of plagioclase in all runs retained their original compositions, with rims having lower An contents towards the melt-troctolite interface (Figure 7c). The difference in core-to-rim compositions of olivine and plagioclase appears consistent with the observed fast diffusion rates of Mg-Fe-Ni in olivine (e.g., Chakraborty, 1997) and slow diffusion of CaAl-NaSi in plagioclase (e.g., Grove et al., 1984; Morse, 1984). To evaluate the control of diffusion on the Mg-Fe equilibrium between melt and olivine at the interface, we modeled the effect of diffusion on the core-to-rim variations of olivine crystals in the troctolite near the reaction interface in run TE1. During the 6 h experimental duration, diffusion should only affect the Fo and Ni contents within ~2 μm of the rim (Figure S2 in Supporting Information). However, even the core compositions of olivine near the interface are in chemical equilibrium with the interface melt for the isothermal runs, suggesting accelerated rate of reequilibration by diffusion-assisted dissolution and reprecipitation. This is consistent with the presence of plagioclase inclusions in olivine crystals (Figure 2b). Therefore, the reaction occurring in the troctolite during the isothermal experiments is as follows:



The relative portions of plagioclase and olivine dissolved in the melt are discussed in Section 4.2.

The isothermal experiments TE1 and TP1 demonstrate that after 6 h of reaction, melt dissolved troctolite around the margins of olivine and plagioclase, forming an interstitial melt phase. In most cooling experiments, clinopyroxene formed around some of the olivine and plagioclase grains of the troctolite during cooling to form the clinopyroxene-bearing troctolite (Figure 3d). In the long duration run TE_Ls, melt-troctolite reaction for 27 h has produced relatively large porosity in the troctolite and interstitial melt phase is present in the entire troctolite section (green in the element map in Figure 3a). Upon cooling, clinopyroxene started to form from this interstitial melt around some of the olivine and plagioclase grains (Figure 3d), and reduced the porosity of the troctolitic mush. The olivine chadacrysts are rounded as a result of earlier dissolution, which is in contrast with the larger olivine grains not enclosed in clinopyroxene (Figure 3d). These observations indicate that the reaction that occurred in the troctolite during the step-cooling experiments included dissolution and reprecipitation of olivine and plagioclase as well as the precipitation of clinopyroxene as the new mineral, following the reaction:



4.2 Quantifying dissolution and reprecipitation

Systematic variations in the reacted melt compositions in runs TE1, TP1 and TE_mush can be used to quantify the dissolution (and reprecipitation) of plagioclase and olivine in the troctolite during melt-mush reaction. We used the reaction in Eq. [1], which includes the roles of both dissolution and reprecipitation of olivine in modifying melt compositions in the isothermal experiments. We neglected plagioclase reprecipitation as a simplification. This is a reasonable

assumption since we observed no olivine relics in plagioclase and mostly quench growth of plagioclase rims. The oxides in the melt that change considerably, such as Al_2O_3 , MgO , TiO_2 , and FeO , are used to calculate the net amount of dissolution. Although experimental study suggested dissolution of plagioclase is ~6 times faster than olivine in basaltic magmas (Donaldson, 1985), the actual dissolution rate of plagioclase to olivine may be lower considering activation enthalphy of dissolution and affinity of the minerals in the melt (Lissenberg & Dick, 2008). In our calculations, we modeled reaction using a range of plagioclase to olivine dissolution ratios (6:1, 3:1, 2:1, and 1:1).

The starting evolved and primitive melt compositions were used to model the assimilation of the starting olivine and plagioclase with varied proportions and the reprecipitation of the olivine at the melt-troctolite interface for each run. The equilibrium between the core compositions of olivine near the interface with melt, which could not be explained by diffusion in 6 hours (Figure S2 in Supporting Information), suggests that the ratio of reprecipitated to dissolved olivine is relatively high. Our model suggests that high ratios (>0.6) would lead to decreasing MgO in melt, inconsistent with melt variations. With the reprecipitated to dissolved olivine ratios in the range 0.4-0.6, the interface melt compositions can be accounted for with dissolved plagioclase/olivine ratios from 2:1 to 1:1. An example is shown in Figure 8 with a reprecipitated to dissolved olivine ratio of 0.5.

5 Geological applications

5.1 Comparison with natural observations

Previous petrologic studies of lower oceanic crust found that relatively primitive cumulates (troctolite, olivine gabbro) are commonly crosscut by more evolved gabbro at fast- (e.g., Hess Deep, ODP Hole 894; Natland & Dick, 1996), slow- (e.g., Kane Megamullion; Dick et al., 2008; Lissenberg & Dick, 2008; Atlantis Massif, Suhr et al., 2008) and ultraslow-spreading ridges (e.g., ODP Hole 735B, Southwest Indian Ridge; Dick et al., 2000). Crystals (both olivine and plagioclase) in MORB are commonly more primitive than those in equilibrium with the host melt (Coogan, 2014), indicating that reaction between a more evolved phenocryst-poor magma and a more primitive crystal-rich mush is common. Microtextures such as poikilitic high-Mg# clinopyroxene with plagioclase and/or olivine chadacrysts, similar to the high-Mg# clinopyroxene produced in the experimental charges (Figure 3d), have been found in natural lower oceanic crust cumulates (e.g., Coogan et al., 2000a; Lissenberg & Dick, 2008; Lissenberg et al., 2013; Sanfilippo et al., 2013, 2019) and crust sections of ophiolites (e.g. Basch et al., 2019; Sanfilippo et al., 2015b). All these observations indicate that reactions of MORB with primitive cumulates, as per our experimental study, are a common process in the lower oceanic crust.

In this section, we compare the compositional variations in melts and minerals in our experimental charges with those observed in samples from lower oceanic crustal cumulates. We emphasize general mineral compositional trends rather than absolute values and ranges, as the latter depend specifically on melt composition, temperature, pressure, duration and melt-rock ratio during melt-mush reaction.

5.1.1 Fo-Ni variations in olivine in natural lower oceanic crust cumulates

Fo and Ni variations in olivine of cumulates have been used as indicators for magma chamber processes (e.g., Coogan, 2014; Rampone et al., 2016; Sanfilippo et al., 2013; Suhr et al.,

2008). Our experiments suggest that primitive mush reacting with variously evolved magma would lead to a decrease in both the Fo and Ni contents of the olivine. Ni contents are predominantly controlled by the change in Ni partition coefficient between evolved and primitive melts. The higher the Mg# of the melt, the lower partition coefficients of Ni in olivine (Hart & Davis, 1978). Thus, the primitive melt in TP1 with higher Mg# would have a lower partition coefficient for Ni in olivine, indicating that reacting with a more primitive melt would decrease the Ni in olivine more rapidly than an evolved melt (Figure 9). Prolonged interaction with evolved melts (run TE_Ls) leads to very low Ni contents ($\text{NiO} < 0.1\%$; Figure 9).

To compare the relative effects of magma differentiation and melt-mush reaction on the Fo vs. Ni correlation of olivine in the cumulates, we modeled olivine compositional variations produced by the fractional crystallization of a primary MORB (ALV0527-001-001, Gale et al., 2013a) using MELTS (Ghiorso & Sack, 1995). As MORB are known to undergo sulfide-saturated differentiation before eruption (e.g., Bézous et al., 2005; Yang et al., 2014), and Ni, as a chalcophile element, is partly controlled by sulfide saturation during magma evolution, we modeled both sulfide-saturated and sulfide-undersaturated fractionation trends. Ni contents in the olivine were calculated with composition- and temperature-dependent K_D for Ni partitioning between olivine and melt (Matzen et al., 2013), and $D_{\text{Ni}}^{\text{sulf/melt}}$ of 500 (Peach et al., 1990) for Ni partitioning between sulfide and melt. Sulfur-saturated differentiation used a silicate to sulfide fractionation ratio of 1000, equivalent to a sulfide segregation rate of ~ 10 ppm per % fractional crystallization as estimated for MORB evolution in Bézous et al. (2005) and Yang et al. (2014). The gentler decreases in Ni for Fo lower than 84 in the modeled fractionation trends is due to the addition of clinopyroxene on the liquidus. In Figure 9, we also plot olivine phenocrysts compositions from MORB, as well as lower oceanic crustal cumulates from fast- (Hess Deep & Pito Deep, East Pacific Rise), slow- (MARK area, Hole 1309D, Mid-Atlantic Ridge) to ultraslow-spreading (Hole 735B, Southwest Indian Ridge) ridges. As demonstrated in Figure 9, a large number of olivines in lower oceanic crustal cumulates and olivine phenocrysts in MORB have both higher and lower NiO at a given Fo content than olivine from both sulfide-saturated and sulfide-undersaturated fractionation models, suggesting that olivine compositional variations in both MORB and cumulates cannot be explained by fractionation alone. Post-crystallization reactions of olivine in cumulates were suggested to have different effects on Fo and Ni contents, which were proposed to account for those olivines with both slightly higher Ni (Coogan, 2014; Suhr et al., 2008), and slightly lower Ni (Sanfilippo et al., 2013) at a given Fo. Our experimental work revealed that Ni variations in olivine after melt-mush reaction would largely depend on the Mg# of the reacted melt. Compared to the olivine from normal fractionation trends before clinopyroxene crystallization, higher Mg# in the primitive melt (run TP1) would result in olivine with lower Ni, while lower Mg# in the evolved melt (run TE1) produced olivine with higher Ni contents at high Fo (>84) in the reacted troctolite. Yet, prolonged reaction with troctolite by the evolved melt in run TE_Ls produced olivine with much lower Ni than the fractionation trends after clinopyroxene crystallization at low Fo. Therefore, variably evolved melts reacting with primitive cumulates could be a possible explanation for the wide range of Ni variations in olivine in both lower oceanic crust cumulates and MORB globally (Figure 9).

5.1.2 Origin of high-Mg# clinopyroxene in the lower oceanic crust

During fractional crystallization at crustal depth (≤ 2 kbar), MORB is not predicted to crystallize clinopyroxene until after significant olivine and plagioclase fractionation (Grove et al., 1992). Therefore, the Mg# of the magma has already dropped considerably when clinopyroxene

441 saturates, with experiments providing an average Mg# of ~83 for the first clinopyroxene
 442 crystallized (Grove, 1990; Grove & Bryan, 1983; Grove et al., 1992; Tormey et al., 1987; Yang et
 443 al., 1996). Nonetheless, high-Mg# clinopyroxene ($\text{Mg\#} \geq 85$) is not uncommon in the lower
 444 oceanic crust, and has been found in the Atlantic (Kane Megamullion (Lissenberg & Dick, 2008);
 445 IODP Hole 1309D in the Atlantis Massif (Drouin et al., 2009; Suhr et al., 2008)), Pacific (Pito
 446 Deep (Perk et al., 2007)) and Indian (ODP Hole 735B (Dick et al., 2002)) oceans. Both high-
 447 pressure crystallization (Elthon, 1987) and melt-mush reaction (Lissenberg & Dick, 2008) have
 448 been invoked to explain such high-Mg# clinopyroxene. Olivine gabbros collected from within 1
 449 km of the base of the sheeted dike complex at Pito Deep contain clinopyroxene with Mg# up to 89
 450 (Perk et al., 2007), demonstrating that Mg-rich clinopyroxene can also crystallize during MORB
 451 differentiation at low pressures.

452 The Mg# variations of clinopyroxene in the melt portions of TE and TP runs mainly depend
 453 on the extent to which olivine crystallization preceded clinopyroxene crystallization. By reaction
 454 with troctolite in TP1, the olivine-saturated primitive melt increased its Mg#, and crystallized
 455 olivine with high Fo (up to 87) as a result (Figure 6). Such early crystallization of magnesian
 456 olivine would deplete the melt in MgO, which explains the relatively low Mg# of clinopyroxene
 457 (~82; Figure 6) formed upon the step cooling of this reacted melt (experiment TP2). In contrast,
 458 the Fe-Mg systematics indicate that olivine crystallization did not precede clinopyroxene during
 459 the crystallization of the evolved melt, even after reaction (experiments TE2, TE_SC and TE_Ls;
 460 Figure 6). The increased Mg# in the melt after reaction, therefore, leads to the formation of high-
 461 Mg# clinopyroxene (Mg# up to 86). Although clinopyroxene crystallization is likely enhanced by
 462 the slightly higher pressure of 0.5 GPa of the experiments compared to typical lower oceanic
 463 crustal conditions (0.1-0.2 GPa), the presence of high-Mg# clinopyroxene in the TE runs but not
 464 in TP runs indicates that the factor controlling high-Mg# clinopyroxene precipitation is not higher
 465 pressure as both runs were at the same pressure. Hence, high-Mg# clinopyroxene is most likely to
 466 form when a relatively evolved, clinopyroxene-saturated melt reacts with primitive cumulates.
 467 This conclusion, which is not sensitive to crystallization pressure, is in keeping with the suggested
 468 formation of high-Mg# clinopyroxene in natural oceanic (Lissenberg & Dick, 2008; Lissenberg &
 469 MacLeod, 2016) and ophiolitic (Basch et al., 2018, 2019; Rampone et al., 2016; Sanfilippo et al.,
 470 2015b) gabbros.

471 The clinopyroxenes crystallized in the (reacted) melt portions of the experiments contain
 472 moderate TiO_2 and Na_2O contents, as is expected from fractional crystallization models (Figure
 473 10). Interstitial clinopyroxene in the troctolite in the step-cooling runs, on the other hand, extend
 474 to very high Na_2O and TiO_2 contents (up to 0.81, and 2.51 wt.%, respectively) with high Mg#
 475 (>83), distinct from the clinopyroxene compositions predicted to form by fractional crystallization
 476 (Figure 10). We infer that these titanium and sodium-rich clinopyroxenes form from evolved
 477 interstitial melts (i.e., high TiO_2) that equilibrated with primitive olivine, and thus acquired high
 478 Mg# (cf. Borghini and Rampone, 2007; Borghini et al., 2018; Lissenberg & Dick, 2008). There
 479 are a significant amount of clinopyroxenes in lower oceanic crustal cumulates with compositional
 480 shifts toward higher Na_2O and TiO_2 at high Mg# relative to the fractionation trend (Figure 10 a,b),
 481 indicating their compositions might have been affected by melt-mush reaction (Lissenberg & Dick,
 482 2008; Lissenberg & MacLeod, 2016; Sanfilippo et al., 2019). Furthermore, clinopyroxene from
 483 some lower crustal sections of ophiolites and layered intrusions have even higher Na_2O and TiO_2
 484 contents (Figure 10 c,d), suggesting an important role for such melt-mush reaction in the formation
 485 of both continental and oceanic cumulates.

5.2 Implications for MORB major element barometry and the origin of high-Al MORB

Major element variations of MORB are commonly used to calculate the pressures at which they underwent (partial) crystallization in the crust prior to eruption (e.g., Danyushevsky et al., 1996; Grove et al., 1992; Herzberg, 2004; Villiger et al., 2007; Wanless & Behn, 2017; Yang et al., 1996). Such calculations depend heavily on the MgO-CaO-Al₂O₃ systematics of the melt with higher pressures resulting from higher Al₂O₃ and/or lower CaO, reflecting the more prominent role of clinopyroxene crystallization at higher pressure (Lissenberg & Dick, 2008). Our experimental results demonstrate that interaction of melts with primitive cumulate minerals modifies melt compositions, with higher Al₂O₃ and MgO after reaction in the isothermal experiments (Figure 4). Such compositional changes of the melt may significantly affect the calculated crystallization pressure. To determine the effect of melt-mush reaction on the calculated crystallization pressure, we applied the parameterization of Herzberg (2004) to the evolved melt compositions in TE1 runs, but note that similar results would be obtained with other MORB major element barometers (Danyushevsky et al., 1996; Grove et al., 1992; Villiger et al., 2007; Yang et al., 1996). We chose the melt compositions which match the criteria proposed in Herzberg (2004) to be saturated in clinopyroxene, olivine and plagioclase ($\text{CaO} < -0.3\text{MgO} + 14.5$). As shown in Figure 11, melt-mush reaction would result in an increase in the calculated crystallization pressures from ~0.1 GPa to above 0.4 GPa, corresponding to an apparent shift in crystallization depth of >12 km. Such a result is consistent with previous predictions by Lissenberg and Dick (2008), who stated that the MgO-CaO-Al₂O₃ relationships of MORB could result from melt-mush reaction instead of polybaric fractional crystallization. Hence, melt-mush reaction significantly affect MORB major-element barometers, resulting in erroneous pressures. It follows that such barometers can only be used reliably if reaction can be ruled out.

High-Al MORB, characterized by high Al₂O₃ and MgO (mostly >8 wt.%), as well as low SiO₂ (e.g. 48 wt. %) and low TiO₂ contents, mostly occur at slow-spreading ridges or close to fracture zones and ridge terminations (e.g., Eason & Sinton, 2006; Gale et al., 2014; Gale et al., 2013b; Langmuir & Bender, 1984; Laubier et al., 2012; Melson & O'Hearn, 1979; Meyzen et al., 2003; Standish et al., 2008; Yang et al., 2017). They are proposed to result from either high-pressure clinopyroxene crystallization (Eason & Sinton, 2006) or melt-cumulate reaction (Danyushevsky et al., 2004; Danyushevsky et al., 2003; Gale et al., 2013b; Kamenetsky et al., 1998; Laubier et al., 2012; Lissenberg & Dick, 2008; Slater et al., 2001; Yang et al., 2017). Our experiments indicate that plagioclase is dissolved more rapidly than olivine, and the dissolution of plagioclase is much faster than its reprecipitation during melt-mush reaction. The preferential dissolution relative to reprecipitation of plagioclase would also result in MORB melts with higher Al₂O₃ contents (Figure 4), which would precipitate plagioclase with higher-An (up to 17 mol% higher as in step-cooling TE runs) upon cooling, indicating melt-mush reaction is a possible mechanism for the formation of high-Al MORB.

6 Conclusions

To investigate the mechanisms and chemical consequences of reaction between basaltic magma and primitive cumulates, we conducted melt-mush reaction experiments by juxtaposing troctolite with either a primitive or an evolved MORB. From our results and comparison to natural data, we draw the following conclusions:

1. Melt-mush reactions proceed through diffusion-assisted dissolution and reprecipitation. The troctolite in the isothermal experiments shows interstitial melt phase after reaction, indicating

melt infiltration and dissolution of plagioclase and olivine with plagioclase/olivine ratios of 2 to 1. Even the cores of olivine crystals in the troctolite at the interface have achieved Mg-Fe equilibrium with the melt, and they contain plagioclase inclusions, neither of which can be accounted for by diffusion on the time scale of the experiments, indicating reprecipitation of olivine during reaction. Furthermore, the troctolite in the step-cooling experiments show both interstitial melt and poikilitic clinopyroxene with rounded olivine and plagioclase chadacrysts, indicating clinopyroxene precipitated upon cooling as reaction product.

2. Through reaction with troctolite, melts became more enriched in MgO and Al₂O₃ and depleted in TiO₂ and Na₂O contents, and crystallized more primitive olivine and plagioclase compared to those crystallized from the starting melts. On the other hand, the troctolite shifted to more evolved compositions to be equilibrated with the melt near the melt-troctolite interface. Olivines in the troctolite have different Fo vs. Ni correlations for different starting melt compositions, resulting from varied Ni partition coefficients with different MgO contents of the melt. Clinopyroxene precipitated in the troctolite has high Mg# (>83) with enriched Na₂O and TiO₂ contents, distinct from those crystallized in the melts. Therefore, high-Mg# clinopyroxene can result from melt-mush reaction, and cannot simply be used as evidence for high-pressure crystallization.

3. The higher MgO and Al₂O₃ contents of reacted melts significantly affect the pressures inferred from MORB major element barometers. The reacted melt yielded higher calculated pressures (~ 0.4 – 0.5 GPa) than that calculated from the starting compositions (~ 0.1 GPa), indicating that major element-based barometers for MORB fractionation can only be used reliably if reaction can be ruled out.

4. The Fo-Ni correlations of olivine, as well as Mg# vs. TiO₂ and Na₂O correlations of clinopyroxene in cumulate rocks can be used to identify the role of melt-mush reaction in the chemical variations of cumulates. By comparison with cumulates from lower oceanic crust, ophiolite and layered intrusion, we propose that melt-mush reaction plays an important role during magma emplacement and transport in crystal mush in both oceanic and continental magma systems.

Acknowledgments

This work was supported by National Programme on Global Change and Air-Sea Interaction (GASI-GEOGE-02), Natural Science Foundation of China (41773025), Strategic Priority Research Program of the Chinese Academy of Sciences (XDB18000000) and China Scholarship Council (AYY). Experimental studies of melt-rock interaction at Brown University have been supported by grants from US National Science Foundation, most recently through EAR-1624516. We thank John Sinton, Benoit Ildefonse and Alberto Saal for providing starting materials, and Matthew Loocke, Duncan Muir, Changming Xing for assistance with the SEM and EMPA analyses. The manuscript benefited greatly from discussions with Xingcheng Liu and Changming Xing. We are grateful to Elisabetta Rampone, Alessio Sanfilippo and Marie Edmonds for careful and constructive comments and editorial handling which significantly improved the manuscript. All data are provided with the paper and in the Supplementary Information tables, and are also available from EarthChem at <http://dx.doi.org/10.1594/IEDA/111370>. This is contribution IS-2739 from GIGCAS.

References

- Ashwal, L. D., Webb, S. J., & Knoper, M. W. (2005). Magmatic stratigraphy in the Bushveld Northern Lobe: continuous geophysical and mineralogical data from the 2950 m Bellevue drillcore. *South African Journal of Geology*, 108(2), 199-232.
- Basch, V., Rampone, E., Crispini, L., Ferrando, C., Ildefonse, B., & Godard, M. (2018). From mantle peridotites to hybrid troctolites: Textural and chemical evolution during melt-rock interaction history (Mt. Maggiore, Corsica, France). *Lithos*, 323, 4-23. doi: 10.1016/j.lithos.2018.02.025
- Basch, V., Rampone, E., Crispini, L., Ferrando, C., Ildefonse, B., & Godard, M. (2019). Multi-stage Reactive Formation of Troctolites in Slow-spreading Oceanic Lithosphere (Erro-Tobbio, Italy): a Combined Field and Petrochemical Study. *Journal of Petrology*.
- Bédard, J., Sparks, R., Renner, R., Cheadle, M., & Hallworth, M. (1988). Peridotite sills and metasomatic gabbros in the Eastern Layered Series of the Rhum complex. *Journal of the Geological Society*, 145(2), 207-224.
- Bédard, J. H. (1991). Cumulate recycling and crustal evolution in the Bay of Islands ophiolite. *The Journal of Geology*, 99(2), 225-249.
- Bennett, E. N., Lissenberg, C. J., & Cashman, K. V. (2019). The significance of plagioclase textures in mid-ocean ridge basalt (Gakkel Ridge, Arctic Ocean). *Contributions to Mineralogy and Petrology*, 174(6), 49.
- Bézos, A., Lorand, J. P., Humler, E., & Gros, M. (2005). Platinum-group element systematics in Mid-Oceanic Ridge basaltic glasses from the Pacific, Atlantic, and Indian Oceans. *Geochimica et Cosmochimica Acta*, 69(10), 2613-2627.
- Bedard, J. H., Hebert, R., Berclaz, A., & Varfalvy, V. (2000). Syntexis and the genesis of lower oceanic crust. *Geological Society of America*, 349, 105-C119.
- Blackman, D. K., Ildefonse, B., John, B. E., Ohara, Y., Miller, D., Abe, N., . . . Awaji, S. (2011). Drilling constraints on lithospheric accretion and evolution at Atlantis Massif, Mid - Atlantic Ridge 30 N. *Journal of Geophysical Research: Solid Earth*, 116(B7).
- Borghini, G., Francomme, J., & Fumagalli, P. (2018). Melt-dunite interactions at 0.5 and 0.7 GPa: experimental constraints on the origin of olivine-rich troctolites. *Lithos*, 323, 44-57.
- Borghini, G., & Rampone, E. (2007). Postcumulus processes in oceanic-type olivine-rich cumulates: the role of trapped melt crystallization versus melt/rock interaction. *Contributions to Mineralogy and Petrology*, 154(6), 619-633. doi: 10.1007/s00410-007-0217-5
- Boudreau, A. (1999). Fluid fluxing of cumulates: the JM reef and associated rocks of the Stillwater Complex, Montana. *Journal of Petrology*, 40(5), 755-772.
- Canales, J. P., Collins, J. A., Escartín, J., & Detrick, R. S. (2000). Seismic structure across the rift valley of the Mid - Atlantic Ridge at 23°20' (MARK area): Implications for crustal accretion processes at slow spreading ridges. *Journal of Geophysical Research: Solid Earth*, 105(B12), 28411-28425.
- Carbotte, S. M., Marjanović, M., Carton, H., Mutter, J. C., Canales, J. P., Nedimović, M. R., . . . Perfit, M. R. (2013). Fine-scale segmentation of the crustal magma reservoir beneath the East Pacific Rise. *Nature Geoscience*, 6(10), 866.
- Cashman, K. V., Sparks, R. S. J., & Blundy, J. D. (2017). VOLCANOLOGY Vertically extensive and unstable magmatic systems: A unified view of igneous processes. *Science*, 355(6331). doi: 10.1126/science.aag3055
- Chakraborty, S. (1997). Rates and mechanisms of Fe - Mg interdiffusion in olivine at 980°–1300° C. *Journal of Geophysical Research: Solid Earth*, 102(B6), 12317-12331.
- Chakraborty, S. (2010). Diffusion coefficients in olivine, wadsleyite and ringwoodite. *Reviews in Mineralogy and Geochemistry*, 72(1), 603-639.
- Coogan, L. (2014). The lower oceanic crust. In K. K. Turekian & H. D. Holland (Eds.), *Treatise on geochemistry* (2nd ed., pp. 497-541): Elsevier.
- Coogan, L., Saunders, A., Kempton, P., & Norry, M. (2000a). Evidence from oceanic gabbros for porous melt migration within a crystal mush beneath the Mid - Atlantic Ridge. *Geochemistry, Geophysics, Geosystems*, 1(9).
- Coogan, L. A., Gillis, K. M., MacLeod, C. J., Thompson, G. M., & Hekinian, R. (2002). Petrology and geochemistry of the lower ocean crust formed at the East Pacific Rise and exposed at Hess Deep: A synthesis and new results. *Geochemistry Geophysics Geosystems*, 3. doi: 10.1029/2001gc000230
- Coogan, L. A., Kempton, P. D., Saunders, A. D., & Norry, M. J. (2000b). Melt aggregation within the crust beneath the Mid-Atlantic Ridge: evidence from plagioclase and clinopyroxene major and trace element compositions. *Earth and Planetary Science Letters*, 176(2), 245-257. doi: 10.1016/s0012-821x(00)00006-6

- Coumans, J. P., Stix, J., Clague, D. A., Minarik, W. G., & Layne, G. D. (2016). Melt-rock interaction near the Moho: evidence from crystal cargo in lavas from near-ridge seamounts. *Geochimica et Cosmochimica Acta*, 191, 139-164.
- Crank, J. (1975). *The mathematics of diffusion*. Clarendon, Oxford, England.
- Crawford, W. C., & Webb, S. C. (2002). Variations in the distribution of magma in the lower crust and at the Moho beneath the East Pacific Rise at 9–10° N. *Earth and Planetary Science Letters*, 203(1), 117-130.
- Crawford, W. C., Webb, S. C., & Hildebrand, J. A. (1999). Constraints on melt in the lower crust and Moho at the East Pacific Rise, 9 degrees 48 ' N, using seafloor compliance measurements. *Journal of Geophysical Research-Solid Earth*, 104(B2), 2923-2939. doi: 10.1029/1998jb900087
- Daines, M., & Kohlstedt, D. (1994). The transition from porous to channelized flow due to melt/rock reaction during melt migration. *Geophysical Research Letters*, 21(2), 145-148.
- Danyushevsky, L., Sobolev, A., & Dmitriev, L. (1996). Estimation of the pressure of crystallization and H₂O content of MORB and BABB glasses: calibration of an empirical technique. *Mineralogy and Petrology*, 57(3-4), 185-204.
- Danyushevsky, L. V., Leslie, R. A. J., Crawford, A. J., & Durance, P. (2004). Melt inclusions in primitive olivine phenocrysts: The role of localized reaction processes in the origin of anomalous compositions. *Journal of Petrology*, 45(12), 2531-2553. doi: 10.1093/petrology/egh080
- Danyushevsky, L. V., Perfit, M. R., Eggins, S. M., & Falloon, T. J. (2003). Crustal origin for coupled 'ultra-depleted' and 'plagioclase' signatures in MORB olivine-hosted melt inclusions: evidence from the Siqueiros Transform Fault, East Pacific Rise. *Contributions to Mineralogy and Petrology*, 144(5), 619-637.
- Dick, H., Natland, J., Alt, J., Bach, W., Bideau, D., Gee, J., . . . Holm, P. (2000). A long in situ section of the lower ocean crust: results of ODP Leg 176 drilling at the Southwest Indian Ridge. *Earth and Planetary Science Letters*, 179(1), 31-51.
- Dick, H. J., Ozawa, K., Meyer, P. S., Niu, Y., Robinson, P. T., Constantin, M., . . . Hirth, G. (2002). 10. Primary silicate mineral chemistry of a 1.5-km section of very slow spreading lower ocean crust: ODP hole 735B, Southwest Indian ridge. *Proceedings of Ocean Drilling Program, Scientific Results*, 000. College Station, TX: *Ocean Drilling Program*, 1-60.
- Dick, H. J., Tivey, M. A., & Tucholke, B. E. (2008). Plutonic foundation of a slow - spreading ridge segment: Oceanic core complex at Kane Megamullion, 23° 30' N, 45° 20' W. *Geochemistry, Geophysics, Geosystems*, 9(5).
- Dohmen, R., & Chakraborty, S. (2007). Fe–Mg diffusion in olivine II: point defect chemistry, change of diffusion mechanisms and a model for calculation of diffusion coefficients in natural olivine. *Physics and Chemistry of Minerals*, 34(6), 409-430.
- Donaldson, C. H. (1985). The rates of dissolution of olivine, plagioclase, and quartz in a basalt melt. *Mineralogical Magazine*, 49(354), 683-693.
- Drouin, M., Godard, M., Ildefonse, B., Bruguier, O., & Garrido, C. J. (2009). Geochemical and petrographic evidence for magmatic impregnation in the oceanic lithosphere at Atlantis Massif, Mid-Atlantic Ridge (IODP Hole U1309D, 30° N). *Chemical Geology*, 264(1), 71-88.
- Dunn, R. A., Toomey, D. R., & Solomon, S. C. (2000). Three - dimensional seismic structure and physical properties of the crust and shallow mantle beneath the East Pacific Rise at 9° 30' N. *Journal of Geophysical Research: Solid Earth*, 105(B10), 23537-23555.
- Eason, D., & Sinton, J. (2006). Origin of high-Al N-MORB by fractional crystallization in the upper mantle beneath the Galápagos Spreading Center. *Earth and Planetary Science Letters*, 252(3), 423-436.
- Elthon, D. (1987). Petrology of gabbroic rocks from the Mid-Cayman Rise Spreading Center. *Journal of Geophysical Research: Solid Earth*, 92(B1), 658-682. doi: 10.1029/JB092iB01p00658
- Gale, A., Dalton, C. A., Langmuir, C. H., Su, Y., & Schilling, J.-G. (2013a). The mean composition of ocean ridge basalts. *Geochemistry, Geophysics, Geosystems*, 14(3), 489-518. doi: 10.1029/2012GC004334
- Gale, A., Langmuir, C. H., & Dalton, C. A. (2014). The global systematics of ocean ridge basalts and their origin. *Journal of Petrology*, 55(6), 1051-1082.
- Gale, A., Laubier, M., Escrig, S., & Langmuir, C. H. (2013b). Constraints on melting processes and plume-ridge interaction from comprehensive study of the FAMOUS and North Famous segments, Mid-Atlantic Ridge. *Earth and Planetary Science Letters*, 365, 209-220. doi: 10.1016/j.epsl.2013.01.022
- Gao, Y., Hoefs, J., Hellebrand, E., von der Handt, A., & Snow, J. E. (2007). Trace element zoning in pyroxenes from ODP Hole 735B gabbros: diffusive exchange or synkinematic crystal fractionation? *Contributions to Mineralogy and Petrology*, 153(4), 429-442.

- Ghiorso, M. S., & Sack, R. O. (1995). Chemical mass transfer in magmatic processes IV. A revised and internally consistent thermodynamic model for the interpolation and extrapolation of liquid-solid equilibria in magmatic systems at elevated temperatures and pressures. *Contributions to Mineralogy and Petrology*, 119(2), 197-212.
- Grove, T. (1990). *Natural and experimental phase relations of lavas from Seroeki volcano*. Paper presented at the Proceedings of the ocean drilling program, Scientific Results.
- Grove, T. L., Baker, M. B., & Kinzler, R. J. (1984). Coupled CaAl-NaSi diffusion in plagioclase feldspar: experiments and applications to cooling rate speedometry. *Geochimica et Cosmochimica Acta*, 48(10), 2113-2121.
- Grove, T. L., & Bryan, W. (1983). Fractionation of pyroxene-phyric MORB at low pressure: an experimental study. *Contributions to Mineralogy and Petrology*, 84(4), 293-309.
- Grove, T. L., Kinzler, R. J., & Bryan, W. B. (1992). Fractionation of mid-ocean ridge basalt (MORB). *Geophysical Monograph Series*, 71, 281-310.
- Gurenko, A. A., & Sobolev, A. V. (2006). Crust-primitive magma interaction beneath neovolcanic rift zone of Iceland recorded in gabbro xenoliths from Midfell, SW Iceland. *Contributions to Mineralogy and Petrology*, 151(5), 495.
- Hébert, R., Constantin, M., & Robinson, P. (1991). Primary mineralogy of Leg 118 gabbroic rocks and their place in the spectrum of oceanic mafic igneous rocks *Proceedings of the Ocean Drilling Program, Scientific Results* (pp. 3-20). College Station, TX: Ocean Drilling Program.
- Hart, S. R., & Davis, K. E. (1978). Nickel partitioning between olivine and silicate melt. *Earth and Planetary Science Letters*, 40(2), 203-219.
- Hellevang, B., & Pedersen, R. B. (2008). Magma ascent and crustal accretion at ultraslow-spreading ridges: constraints from plagioclase ultraphyric basalts from the Arctic mid-ocean ridge. *Journal of Petrology*, 49(2), 267-294.
- Herzberg, C. (2004). Partial crystallization of mid-ocean ridge basalts in the crust and mantle. *Journal of Petrology*, 45(12), 2389-2405. doi: 10.1093/petrology/egh040
- Irvine, N. (1980). Magmatic infiltration metasomatism, double diffusive fractional crystallization, and adcumulus growth in the Muskox intrusion and other layered intrusions. *Physics of magmatic processes*.
- Kamenetsky, V. S., Eggins, S. M., Crawford, A. J., Green, D. H., Gasparon, M., & Falloon, T. J. (1998). Calcic melt inclusions in primitive olivine at 43° N MAR: evidence for melt-rock reaction/melting involving clinopyroxene-rich lithologies during MORB generation. *Earth and Planetary Science Letters*, 160(1), 115-132.
- Koleszar, A., Saal, A., Hauri, E., Nagle, A., Liang, Y., & Kurz, M. (2009). The volatile contents of the Galapagos plume; evidence for H₂O and F open system behavior in melt inclusions. *Earth and Planetary Science Letters*, 287(3), 442-452.
- Kvassnes, A. J., & Grove, T. L. (2008). How partial melts of mafic lower crust affect ascending magmas at oceanic ridges. *Contributions to Mineralogy and Petrology*, 156(1), 49-71.
- Lambart, S., Laporte, D., & Schiano, P. (2009). An experimental study of focused magma transport and basalt-peridotite interactions beneath mid-ocean ridges: implications for the generation of primitive MORB compositions. *Contributions to Mineralogy and Petrology*, 157(4), 429-451.
- Lange, A. E., Nielsen, R. L., Tepley III, F. J., & Kent, A. J. (2013). The petrogenesis of plagioclase - phyric basalts at mid - ocean ridges. *Geochemistry, Geophysics, Geosystems*, 14(8), 3282-3296.
- Langmuir, C., Klein, E., & Plank, T. (1992). Petrological systematics of mid-ocean ridge basalts: Constraints on melt generation beneath ocean ridges. *Geophysical Monograph Series*, 71, 183-280.
- Langmuir, C. H., & Bender, J. F. (1984). The geochemistry of oceanic basalts in the vicinity of transform faults: observations and implications. *Earth and Planetary Science Letters*, 69(1), 107-127.
- Laubier, M., Gale, A., & Langmuir, C. H. (2012). Melting and Crustal Processes at the FAMOUS Segment (Mid-Atlantic Ridge): New Insights from Olivine-hosted Melt Inclusions from Multiple Samples. *Journal of Petrology*.
- Leuthold, J., Blundy, J. D., & Brooker, R. A. (2015). Experimental petrology constraints on the recycling of mafic cumulate: a focus on Cr-spinel from the Rum Eastern Layered Intrusion, Scotland. *Contributions to Mineralogy and Petrology*, 170(2), 12.
- Leuthold, J., Lissenberg, C. J., O'Driscoll, B., Karakas, O., Falloon, T., Klimentyeva, D. N., & Ulmer, P. (2018). Partial melting of lower oceanic crust gabbro: constraints from poikilitic clinopyroxene primocrysts. *Frontiers in Earth Science*, 6, 15.

- Leuthold, J., Müntener, O., Baumgartner, L. P., & Putlitz, B. (2014). Petrological constraints on the recycling of mafic crystal mushes and intrusion of braided sills in the Torres del Paine mafic complex (Patagonia). *Journal of Petrology*, 55(5), 917-949.
- Lissenberg, C. J., & Dick, H. J. B. (2008). Melt-rock reaction in the lower oceanic crust and its implications for the genesis of mid-ocean ridge basalt. *Earth and Planetary Science Letters*, 271(1-4), 311-325. doi: 10.1016/j.epsl.2008.04.023
- Lissenberg, C. J., & MacLeod, C. J. (2016). A Reactive Porous Flow Control on Mid-ocean Ridge Magmatic Evolution. *Journal of Petrology*, 57(11-12), 2195-2219. doi: 10.1093/petrology/egw074
- Lissenberg, C. J., MacLeod, C. J., Howard, K. A., & Godard, M. (2013). Pervasive reactive melt migration through fast-spreading lower oceanic crust (Hess Deep, equatorial Pacific Ocean). *Earth and Planetary Science Letters*, 361(0), 436-447. doi: <http://dx.doi.org/10.1016/j.epsl.2012.11.012>
- Llovet, X., & Galan, G. (2003). Correction of secondary X-ray fluorescence near grain boundaries in electron microprobe analysis: Application to thermobarometry of spinel lherzolites. *American Mineralogist*, 88(1), 121-130.
- Mathez, E. (1995). Magmatic metasomatism and formation of the Merensky reef, Bushveld Complex. *Contributions to Mineralogy and Petrology*, 119(2-3), 277-286.
- Matzen, A. K., Baker, M. B., Beckett, J. R., & Stolper, E. M. (2013). The temperature and pressure dependence of nickel partitioning between olivine and silicate melt. *Journal of Petrology*, 54(12), 2521-2545.
- McBirney, A. R., & Sonnenthal, E. L. (1990). Metasomatic replacement in the Skaergaard Intrusion, East Greenland: preliminary observations. *Chemical Geology*, 88(3-4), 245-260.
- Melson, W. G., & O'Hearn, T. (1979). Basaltic Glass Erupted Along the Mid - Atlantic Ridge Between 0 - 37° N: Relationships Between Composition and Latitude. *Deep Drilling Results in the Atlantic Ocean: Ocean Crust*, 249-261.
- Meyer, P. S., Dick, H. J., & Thompson, G. (1989). Cumulate gabbros from the Southwest Indian Ridge, 54 S-7 16' E: Implications for magmatic processes at a slow spreading ridge. *Contributions to Mineralogy and Petrology*, 103(1), 44-63.
- Meyzen, C. M., Toplis, M. J., Humler, E., Ludden, J. N., & Mevel, C. (2003). A discontinuity in mantle composition beneath the southwest Indian ridge. *Nature*, 421(6924), 731-733. doi: 10.1038/nature01424
- Miller, D., Abratis, M., Christie, D., Drouin, M., Godard, M., Ildefonse, B., . . . Suzuki, Y. (2009). Data report: microprobe analyses of primary mineral phases from Site U1309, Atlantis Massif, IODP Expedition 304/305. *Proceedings of IODP*, 304, 305.
- Moore, A., Coogan, L., Costa, F., & Perfit, M. (2014). Primitive melt replenishment and crystal-mush disaggregation in the weeks preceding the 2005–2006 eruption 9° 50' N, EPR. *Earth and Planetary Science Letters*, 403, 15-26.
- Morgan, Z., & Liang, Y. (2003). An experimental and numerical study of the kinetics of harzburgite reactive dissolution with applications to dunite dike formation. *Earth and Planetary Science Letters*, 214(1-2), 59-74.
- Morgan, Z., & Liang, Y. (2005). An experimental study of the kinetics of lherzolite reactive dissolution with applications to melt channel formation. *Contributions to Mineralogy and Petrology*, 150(4), 369-385.
- Morse, S. (1984). Cation diffusion in plagioclase feldspar. *Science*, 225(4661), 504-505.
- Namur, O., Humphreys, M. C., & Holness, M. B. (2013). Lateral reactive infiltration in a vertical gabbroic crystal mush, Skaergaard intrusion, East Greenland. *Journal of Petrology*, 54(5), 985-1016.
- Natland, J. H., & Dick, H. J. (1996). *Melt migration through high-level gabbroic cumulates of the East Pacific Rise at Hess Deep: the origin of magma lenses and the deep crustal structure of fast-spreading ridges*. Paper presented at the Proceedings-Ocean Drilling Program Scientific Results.
- Pan, Y., & Batiza, R. (2002). Mid - ocean ridge magma chamber processes: Constraints from olivine zonation in lavas from the East Pacific Rise at 9° 30' N and 10° 30' N. *Journal of Geophysical Research: Solid Earth*, 107(B1), ECV 9-1-ECV 9-13.
- Pan, Y., & Batiza, R. (2003). Magmatic processes under mid - ocean ridges: A detailed mineralogic study of lavas from East Pacific Rise 9° 30' N, 10° 30' N, and 11° 20' N. *Geochemistry, Geophysics, Geosystems*, 4(11).
- Pang, K.-N., Li, C., Zhou, M.-F., & Ripley, E. M. (2009). Mineral compositional constraints on petrogenesis and oxide ore genesis of the late Permian Panzhihua layered gabbroic intrusion, SW China. *Lithos*, 110(1-4), 199-214.

- Peach, C. L., Mathez, E. A., & Keays, R. R. (1990). Sulfide melt silicate melt distribution coefficients for noble metals and other chalcophile elements as deduced from MORB: Implications for partial melting. *Geochimica et Cosmochimica Acta*, 54(12), 3379-3389.
- Perk, N. W., Coogan, L. A., Karson, J. A., Klein, E. M., & Hanna, H. D. (2007). Petrology and geochemistry of primitive lower oceanic crust from Pito Deep: implications for the accretion of the lower crust at the Southern East Pacific Rise. *Contributions to Mineralogy and Petrology*, 154(5), 575-590.
- Rampone, E., Borghini, G., Godard, M., Ildefonse, B., Crispini, L., & Fumagalli, P. (2016). Melt/rock reaction at oceanic peridotite/gabbro transition as revealed by trace element chemistry of olivine. *Geochimica et Cosmochimica Acta*, 190, 309-331. doi: 10.1016/j.gca.2016.06.029
- Ridley, W. I., Perfit, M. R., Smith, M. C., & Fornari, D. J. (2006). Magmatic processes in developing oceanic crust revealed in a cumulate xenolith collected at the East Pacific Rise, 9°50N. *Geochemistry, Geophysics, Geosystems*, 7(12), Q12O04. doi: 10.1029/2006gc001316
- Roeder, P., & Emslie, R. F. (1970). Olivine-liquid equilibrium. *Contributions to Mineralogy and Petrology*, 29(4), 275-289.
- Ross, K., & Elthon, D. (1997). Cumulus and postcumulus crystallization in the oceanic crust: major-and trace-element geochemistry of Leg 153 gabbroic rocks *Proceedings-Ocean Drilling Program Scientific Results*. College Station, TX: Ocean Drilling Program.
- Sanfilippo, A., Dick, H. J., Marschall, H. R., Lissenberg, C. J., & Urann, B. (2019). Emplacement and High - Temperature Evolution of Gabbros of the 16.5° N Oceanic Core Complexes (Mid - Atlantic Ridge): Insights Into the Compositional Variability of the Lower Oceanic Crust. *Geochemistry, Geophysics, Geosystems*, 20(1), 46-66.
- Sanfilippo, A., Dick, H. J. B., & Ohara, Y. (2013). Melt-Rock Reaction in the Mantle: Mantle Troctolites from the Parece Vela Ancient Back-Arc Spreading Center. *Journal of Petrology*, 54(5), 861-885. doi: 10.1093/petrology/egs089
- Sanfilippo, A., Morishita, T., Kumagai, H., Nakamura, K., Okino, K., Hara, K., Arai, S. (2015a). Hybrid troctolites from mid-ocean ridges: inherited mantle in the lower crust. *Lithos*, 232, 124-130. doi: 10.1016/j.lithos.2015.06.025
- Sanfilippo, A., Tribuzio, R., Tiepolo, M., & Berno, D. (2015b). Reactive flow as dominant evolution process in the lowermost oceanic crust: evidence from olivine of the Pineto ophiolite (Corsica). *Contributions to Mineralogy and Petrology*, 170(4). doi: 10.1007/s00410-015-1194-8
- Saper, L., & Liang, Y. (2014). Formation of plagioclase-bearing peridotite and plagioclase-bearing wehrlite and gabbro suite through reactive crystallization: an experimental study. *Contributions to Mineralogy and Petrology*, 167(3). doi: 10.1007/s00410-014-0985-7
- Seher, T., Crawford, W. C., Singh, S. C., Cannat, M., Combier, V., & Dusunur, D. (2010). Crustal velocity structure of the Lucky Strike segment of the Mid - Atlantic Ridge at 37 N from seismic refraction measurements. *Journal of Geophysical Research: Solid Earth*, 115(B3).
- Sisson, T., & Grove, T. (1993). Experimental investigations of the role of H₂O in calc-alkaline differentiation and subduction zone magmatism. *Contributions to Mineralogy and Petrology*, 113(2), 143-166.
- Slater, L., McKenzie, D., GRÖNVOLD, K., & Shimizu, N. (2001). Melt generation and movement beneath Theistareykir, NE Iceland. *Journal of Petrology*, 42(2), 321-354.
- Solano, J., Jackson, M., Sparks, R., & Blundy, J. (2014). Evolution of major and trace element composition during melt migration through crystalline mush: Implications for chemical differentiation in the crust. *American Journal of Science*, 314(5), 895-939.
- Standish, J. J., Dick, H. J. B., Michael, P. J., Melson, W. G., & O'Hearn, T. (2008). MORB generation beneath the ultraslow spreading Southwest Indian Ridge (9-25 degrees E): Major element chemistry and the importance of process versus source. *Geochemistry Geophysics Geosystems*, 9. doi: Q0500410.1029/2008gc001959
- Suhr, G., Hellebrand, E., Johnson, K., & Brunelli, D. (2008). Stacked gabbro units and intervening mantle: A detailed look at a section of IODP Leg 305, Hole U1309D. *Geochemistry, Geophysics, Geosystems*, 9(10).
- Tormey, D., Grove, T. L., & Bryan, W. (1987). Experimental petrology of normal MORB near the Kane Fracture Zone: 22–25 N, mid-Atlantic ridge. *Contributions to Mineralogy and Petrology*, 96(2), 121-139.
- Tursack, E., & Liang, Y. (2012). A comparative study of melt-rock reactions in the mantle: laboratory dissolution experiments and geological field observations. *Contributions to Mineralogy and Petrology*, 163(5), 861-876. doi: 10.1007/s00410-011-0703-7
- Ulmer, P., & Luth, R. W. (1991). The graphite-COH fluid equilibrium in P, T, fO₂ space. *Contributions to Mineralogy and Petrology*, 106(3), 265-272.
- Van Den Bleeken, G., Müntener, O., & Ulmer, P. (2010). Reaction processes between tholeiitic melt and residual

- peridotite in the uppermost mantle: An experimental study at 0–8 GPa. *Journal of Petrology*, 51(1-2), 153-183.
- Van den Bleeken, G., Müntener, O., & Ulmer, P. (2011). Melt variability in percolated peridotite: an experimental study applied to reactive migration of tholeiitic basalt in the upper mantle. *Contributions to Mineralogy and Petrology*, 161(6), 921-945.
- Vera, E., Mutter, J., Buhl, P., Orcutt, J., Harding, A., Kappus, M., . . . Brocher, T. (1990). The structure of 0 - to 0.2 - my - old oceanic crust at 9° N on the East Pacific Rise from expanded spread profiles. *Journal of Geophysical Research: Solid Earth*, 95(B10), 15529-15556.
- Villiger, S., Müntener, O., & Ulmer, P. (2007). Crystallization pressures of mid - ocean ridge basalts derived from major element variations of glasses from equilibrium and fractional crystallization experiments. *Journal of Geophysical Research: Solid Earth*, 112(B1).
- Wang, C., Liang, Y., Xu, W., & Dygert, N. (2013). Effect of melt composition on basalt and peridotite interaction: laboratory dissolution experiments with applications to mineral compositional variations in mantle xenoliths from the North China Craton. *Contributions to Mineralogy and Petrology*, 166(5), 1469-1488.
- Wanless, V. D., & Behn, M. D. (2017). Spreading rate-dependent variations in crystallization along the global mid-ocean ridge system. *Geochemistry Geophysics Geosystems*, 18(8), 3016-3033. doi: 10.1002/2017gc006924
- Yamazaki, S., Neo, N., & Miyashita, S. (2009). Data report: whole-rock major and trace elements and mineral compositions of the sheeted dike–gabbro transition in ODP Hole 1256D *Proceedings of Ocean Drilling Program, Scientific Results* (pp. 309-312). College Station, TX: Ocean Drilling Program.
- Yang, A., Zhao, T. P., Zhou, M. F., & Deng, X. G. (2017). Isotopically enriched N - MORB: A new geochemical signature of off - axis plume - ridge interaction—A case study at 50° 28' E, Southwest Indian Ridge. *Journal of Geophysical Research: Solid Earth*, 122(1), 191-213.
- Yang, A. Y., Zhou, M.-F., Zhao, T.-P., Deng, X.-G., Qi, L., & Xu, J.-F. (2014). Chalcophile elemental compositions of MORBs from the ultraslow-spreading Southwest Indian Ridge and controls of lithospheric structure on S-saturated differentiation. *Chemical Geology*, 382(0), 1-13. doi: <http://dx.doi.org/10.1016/j.chemgeo.2014.05.019>
- Yang, H.-J., Kinzler, R. J., & Grove, T. (1996). Experiments and models of anhydrous, basaltic olivine-plagioclase-augite saturated melts from 0.001 to 10 kbar. *Contributions to Mineralogy and Petrology*, 124(1), 1-18.

Figure Captions

Figure 1. Setup and cooling history of all the experimental charges in this study. Time = 0 marks the beginning of the experiment, when the target temperatures of 1180°C and 1200 °C were reached. See the text in Section 3 for detailed description of each run.

Figure 2. Texture of isothermal run TE1. a) Backscattered electron (BSE) image for run TE1 showing interstitial melt phases in the troctolite (~5% in panel 2b, and almost none in 2d), forming a melting-infiltration zone in the troctolite. b) shows plagioclase (pl) included in euhedral olivine (ol) grains, indicating that the troctolite underwent dissolution-reprecipitation reactions. c) interstitial melt phases occur mainly as thin film surrounding plagioclase, whereas d) at the bottom of the troctolite section without interstitial melt phase, plagioclase boundaries are obscure. e) Ti element map of the 400 µm melt infiltration zone in run TE1 highlights the melt phase in green, showing more interstitial melt in the troctolite closer to the melt-troctolite interface. The locations of a) and e) are shown in the full BSE image of TE1 in Figure S1a in Supporting Information

Figure 3. Texture of long duration step-cooling run TE_Ls. a) Element map showing the texture of upper gabbro and lower troctolite. Troctolite section is composed of plagioclase (pl, dark grey color representing low-Na plagioclase in the troctolite) and olivine (ol, bright red color) with interstitial clinopyroxene (cpx, darker red color surrounding olivine and plagioclase) in b), and interstitial melt (green color) in c). Plagioclase in the gabbro has a lighter blue color due to higher Na contents in the plagioclase crystallizing from the melt compared to those in the troctolite. d) backscattered electron image for poikilitic clinopyroxene (outlined with yellow dashed curve) enclosing plagioclase and olivine chadacrysts (outlined with white curves and labeled with white fonts) in the troctolite section. Plagioclase relict hosted in olivine suggests reprecipitated olivine grew over resorbed plagioclase. The olivine chadacrysts in the poikilitic clinopyroxene are rounded as a result of dissolution, in contrast with the larger olivine grains (labeled with yellow fonts) not enclosed in clinopyroxene

Figure 4. Plots of Mg# (defined as mole fractions of $100 \cdot \text{MgO}/(\text{MgO} + \text{FeO}^{\text{T}})$) and oxides in melt as a function of distance away from the melt-troctolite interface in runs TE1, TP1, and TE_mush. Logarithmic scales were used to plot the TiO_2 variations in run TE1 and TP1. Solid lines correspond to the starting melt compositions. Clinopyroxene is present in the upper part of melt phase in run TE1, represented by the area to the right of the dashed line in a) and b). Interstitial melt compositions in the troctolite were also plotted for TE_mush, shown to the left of the dashed line in e) and f)

Figure 5. Plot of Mg# in melt and fosterite content of olivine (Fo) in the troctolite near interface for runs TE1, TE_mush and TP1. Grey and black dashed curves indicate equilibrated melt and olivine compositions with K_D of 0.30 ± 0.03 (e.g., Roeder & Emslie, 1970). Grey circle and triangle represent the starting melt and olivine compositions of run TE1, TE_mush and TP1, respectively. Blue circle, purple diamond and orange triangles represent melt and olivine compositions near the melt-troctolite interface for the three runs after reaction, and they are plotted within the field defined by K_D of 0.30 ± 0.03 , suggesting chemical equilibration was achieved at the interface after reaction. Olivine in both the troctolite (tr) and melt (m) are plotted for run TP1.

Figure 6. Plot of the highest Mg# of clinopyroxene and Fo of olivine in the gabbro sections of each step-cooling run. Grey shaded area represents clinopyroxene and olivine compositions in equilibrium, defined by the Fe-Mg exchange equilibrium constant $K_D^{\text{cpx/melt}}$ from 0.23-0.26 (Grove & Bryan, 1983; Sisson & Grove, 1993) and $K_D^{\text{ol/melt}}$ from 0.27-0.33 (e.g., Roeder & Emslie, 1970). Experimental charges plotted below the equilibrium field indicate olivine crystallized early than clinopyroxene and vice versa, demonstrating the first phase to crystallize in the gabbro sections changed from cotectic clinopyroxene and olivine to olivine in TP runs (shown by the orange line with an arrow), and from clinopyroxene to cotectic olivine and clinopyroxene in TE runs

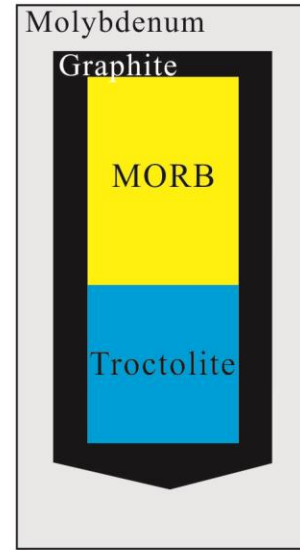
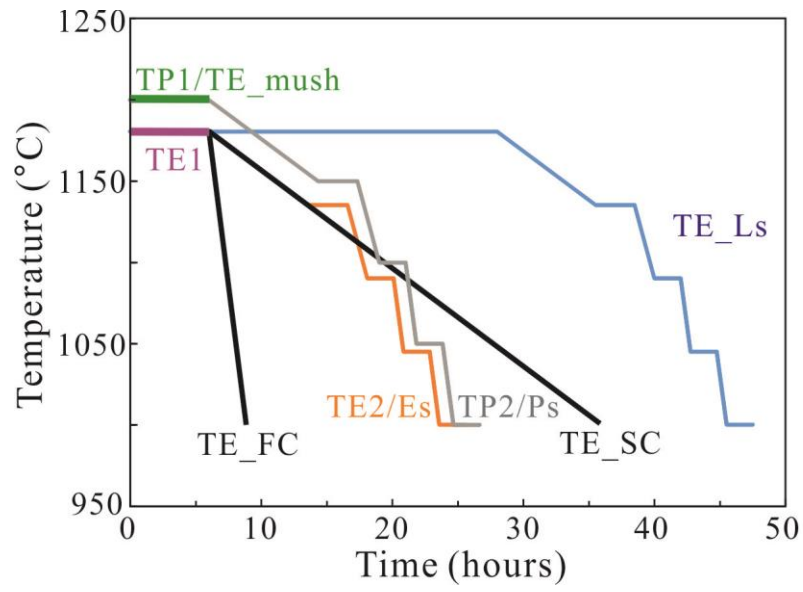
Figure 7. Plots of a) Fo and b) NiO contents in the olivine cores for runs TP1, TE1 and TE_Ls and c) Anorthite (An) in the cores and rims of plagioclase for run TE1 in the troctolite as a function of distance away from the melt-troctolite interface. Rim analyses were not plotted as most of the olivine are too small to yield good-quality data on the rims due to the possible effect of secondary fluorescence contamination (e.g., Llovet & Galan, 2003). Grey shaded fields represent the starting olivine and plagioclase compositions

Figure 8. Modeling of melt compositional variations during melt-troctolite reaction in runs TE1 (a-c), TP1 (d-f), and TE_mush (g-i). Grey circle and triangle represent the starting compositions of evolved and primitive melts, respectively. Black lines are for reaction models with the actual mineral proportions in the troctolite, and lines with other colors show different dissolved plagioclase to olivine ratios as noted. Marks on the modeled lines denote the relative percentage of assimilants (in 5% increments). Different symbols indicate varied distances from the analyzed melt spots to the melt-troctolite interface.

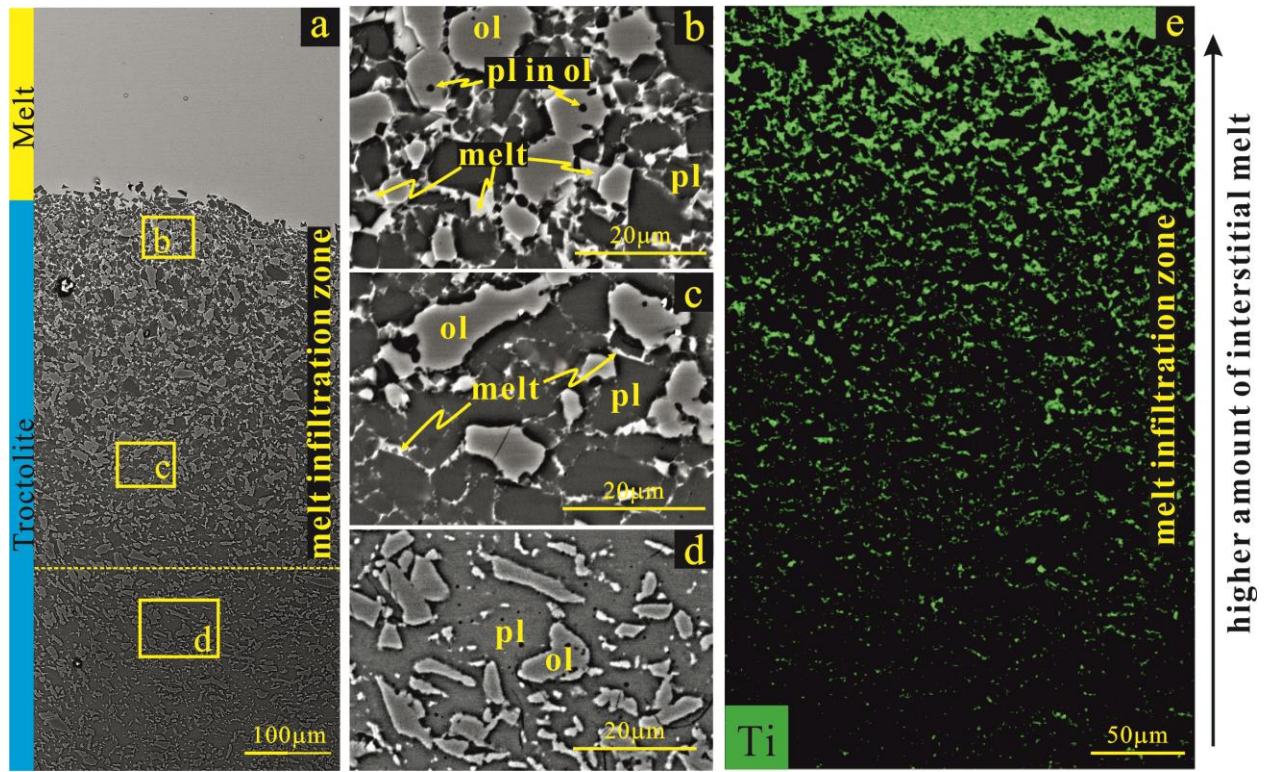
Figure 9. Variation in olivine Fo and Ni contents in both melt/gabbro and troctolite (tr.) sections in the experimental charges. Light and dark grey dots represent olivine in global lower oceanic cumulates (data are from Dick et al., 2002; Hébert et al., 1991; Lissenberg et al., 2013; Miller et al., 2009; Natland & Dick, 1996; Perk et al., 2007; Ross & Elthon, 1997; Suhr et al., 2008; Yamazaki et al., 2009) and olivine phenocrysts in MORB (from PetDB database), respectively. Orange dots represent sulfur-undersaturated fractionation trend of a primary MORB (ALV0527-001-001, Gale et al., 2013a). From this melt olivine, followed by plagioclase and clinopyroxene is removed by fractional crystallization, and each dot represents a 1°C temperature step, modeled using MELTS (Ghiorso & Sack, 1995). Blue dots represent the sulfur-saturated fractionation trend from the same melt with a silicate/sulfide fractionation ratio of 1000 based on the sulfide segregation rates during MORB differentiation from Bézous et al. (2005) and Yang et al. (2014).

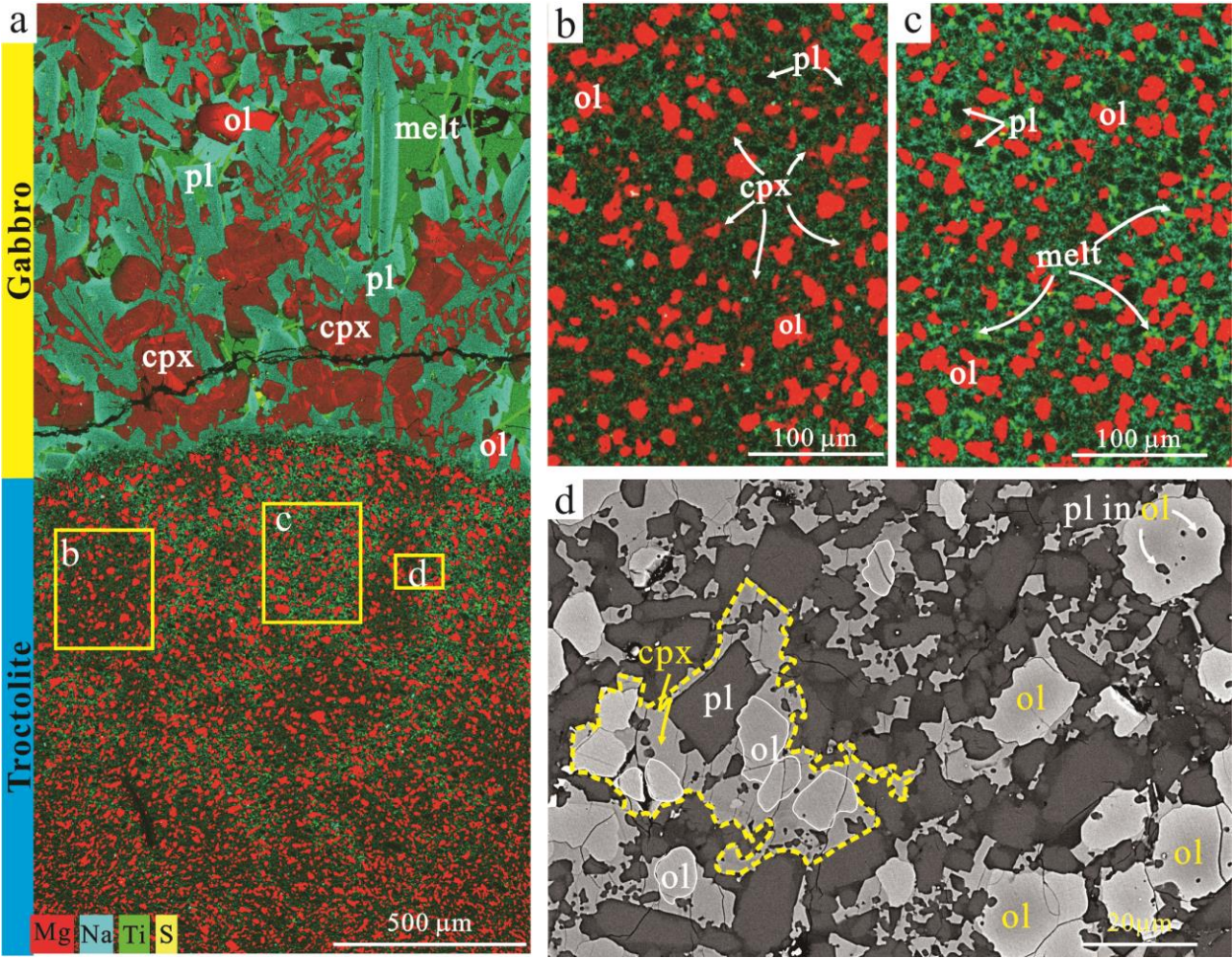
Figure 10. Variations in TiO₂ and Na₂O contents versus Mg# of clinopyroxene in both melt/gabbro (m) and troctolite (tr) sections in runs TE and TP. Grey dots represent clinopyroxene in a&b) lower oceanic cumulates (data are from Coogan et al., 2002; Coogan et al., 2000b; Dick et al., 2002; Hébert et al., 1991; Lissenberg et al., 2013; Miller et al., 2009; Natland & Dick, 1996; Perk et al., 2007; Ross & Elthon, 1997; Sanfilippo et al., 2019; Suhr et al., 2008; Yamazaki et al., 2009), and c&d) Erro-Tobbio ophiolite (Basch et al., 2019) and Panzhihua layered intrusion (Pang et al., 2009). Black dots represent fractional crystallization trend of the same MORB magma as described in Figure 9. Arrows show the effect of melt-mush reaction on the clinopyroxene compositions

Figure 11. Plot of fractionation pressures calculated using the method in Herzberg (2004) as a function of distance away from the melt-troctolite interface in run TE1. Melt compositions that match the criteria of $\text{CaO} < -0.3\text{MgO} + 14.5$ as proposed in Herzberg (2004) were chosen for calculation. Orange arrow shows the trend for the effect of melt-mush reaction on the calculated pressures. Grey line indicates the calculated pressure for the starting evolved melt composition as listed in Table 1

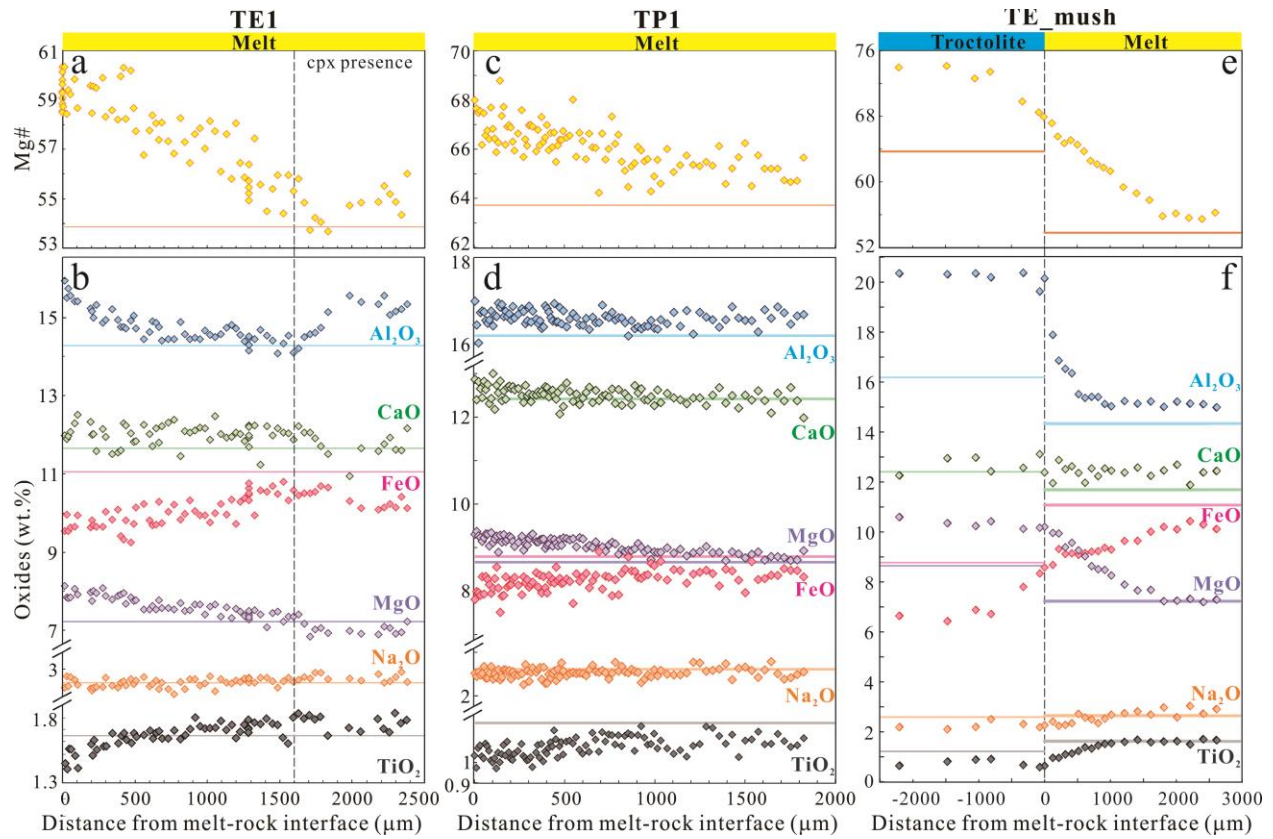


969
970



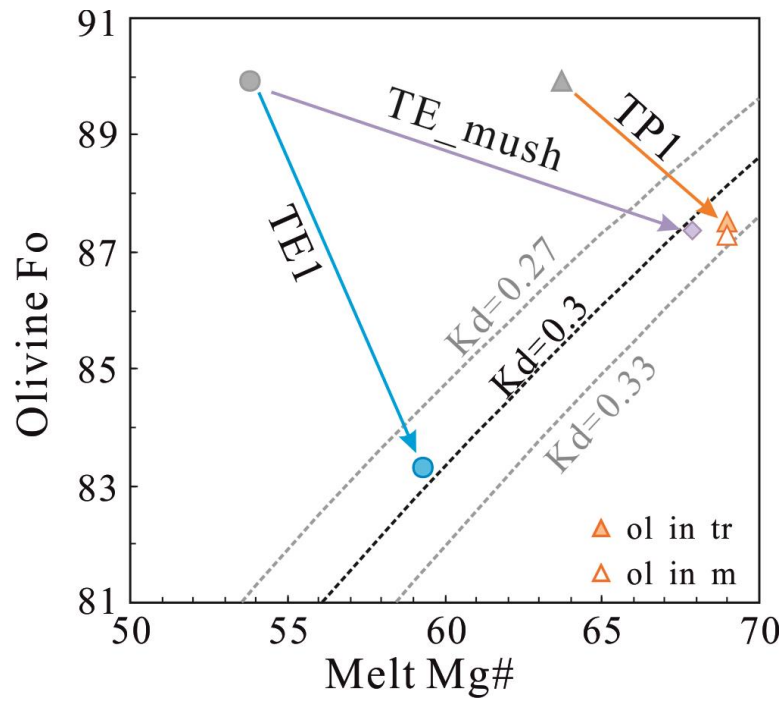


972
973

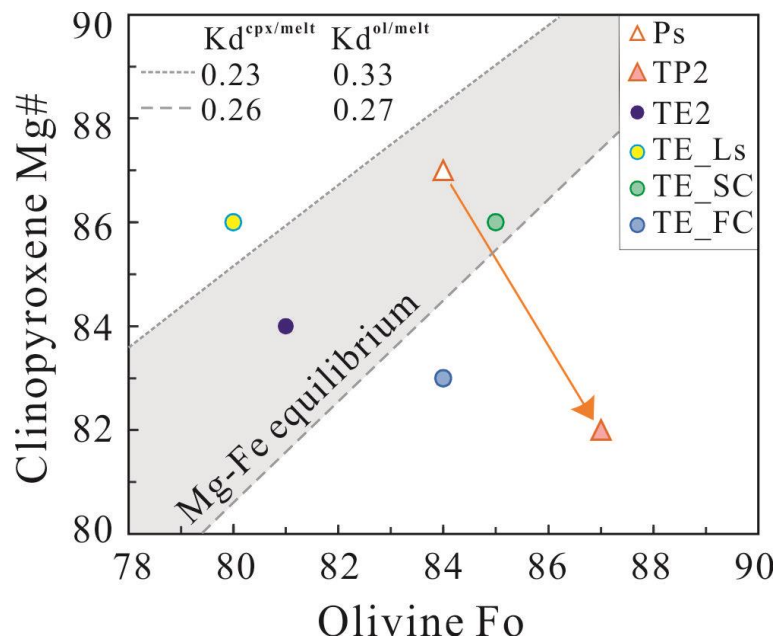


974

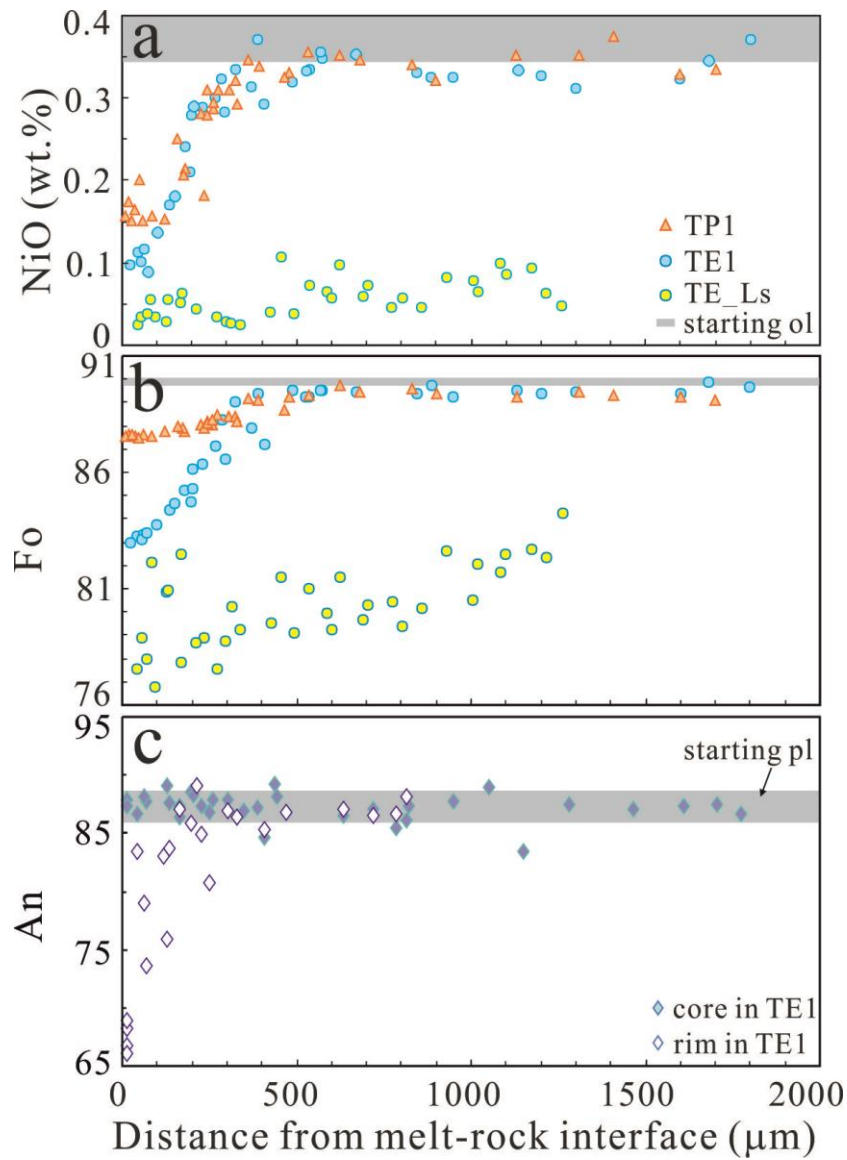
975

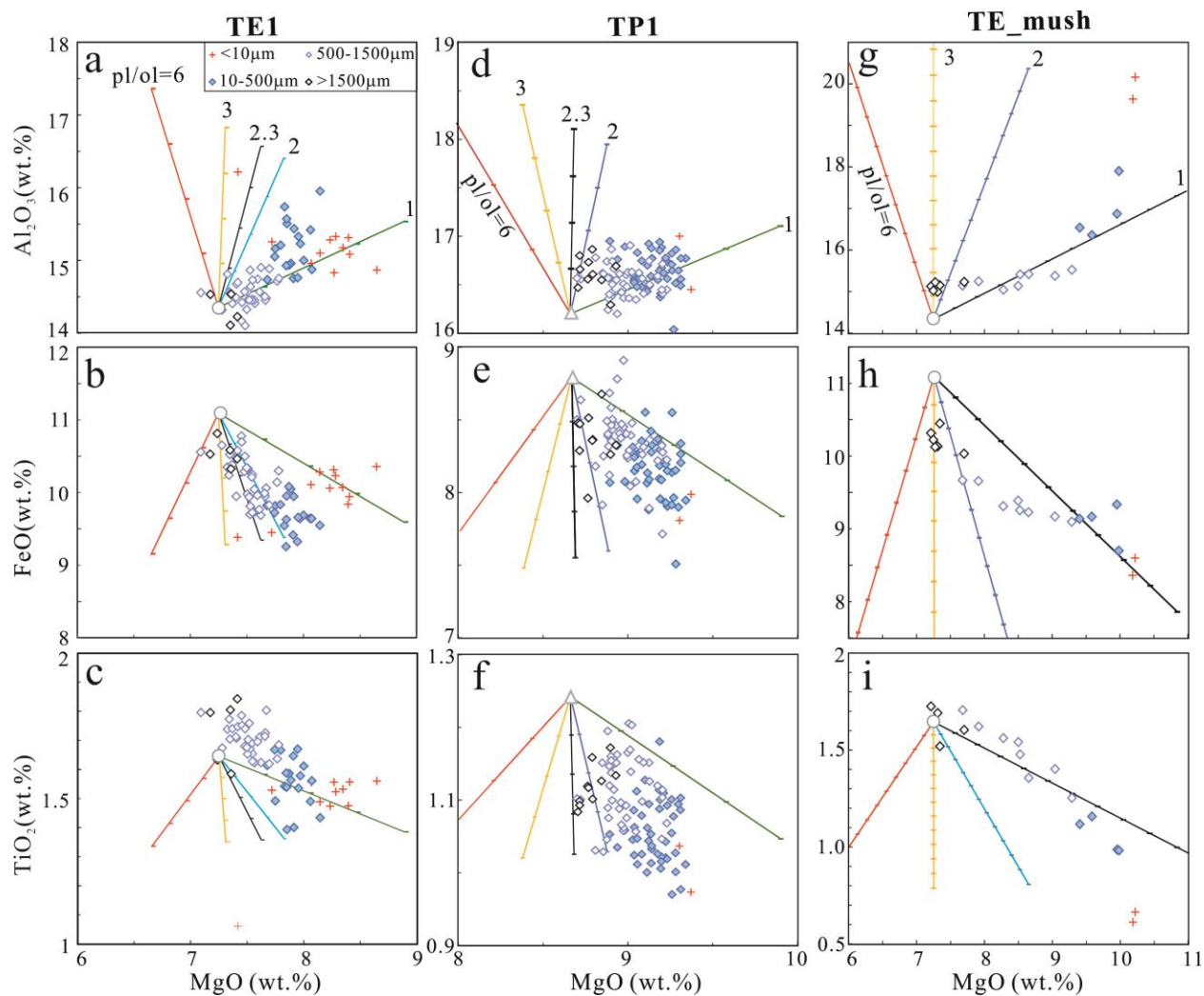


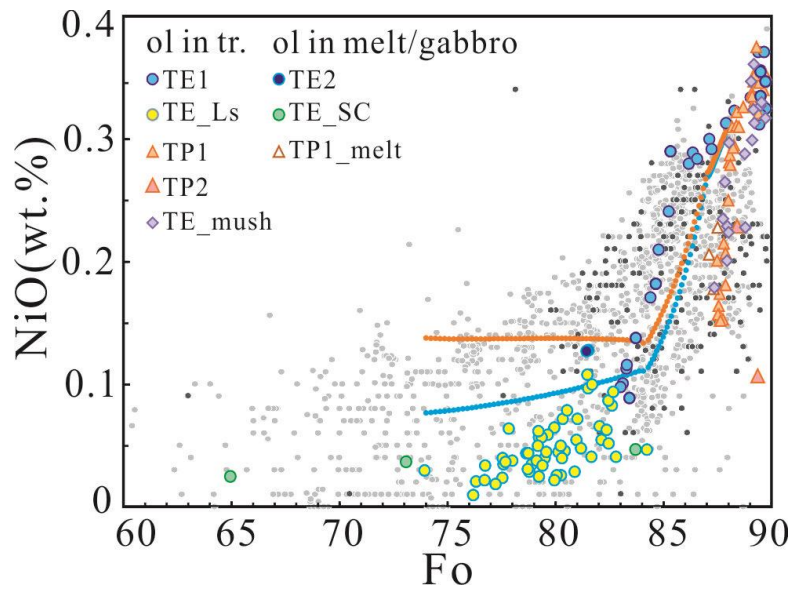
976
977



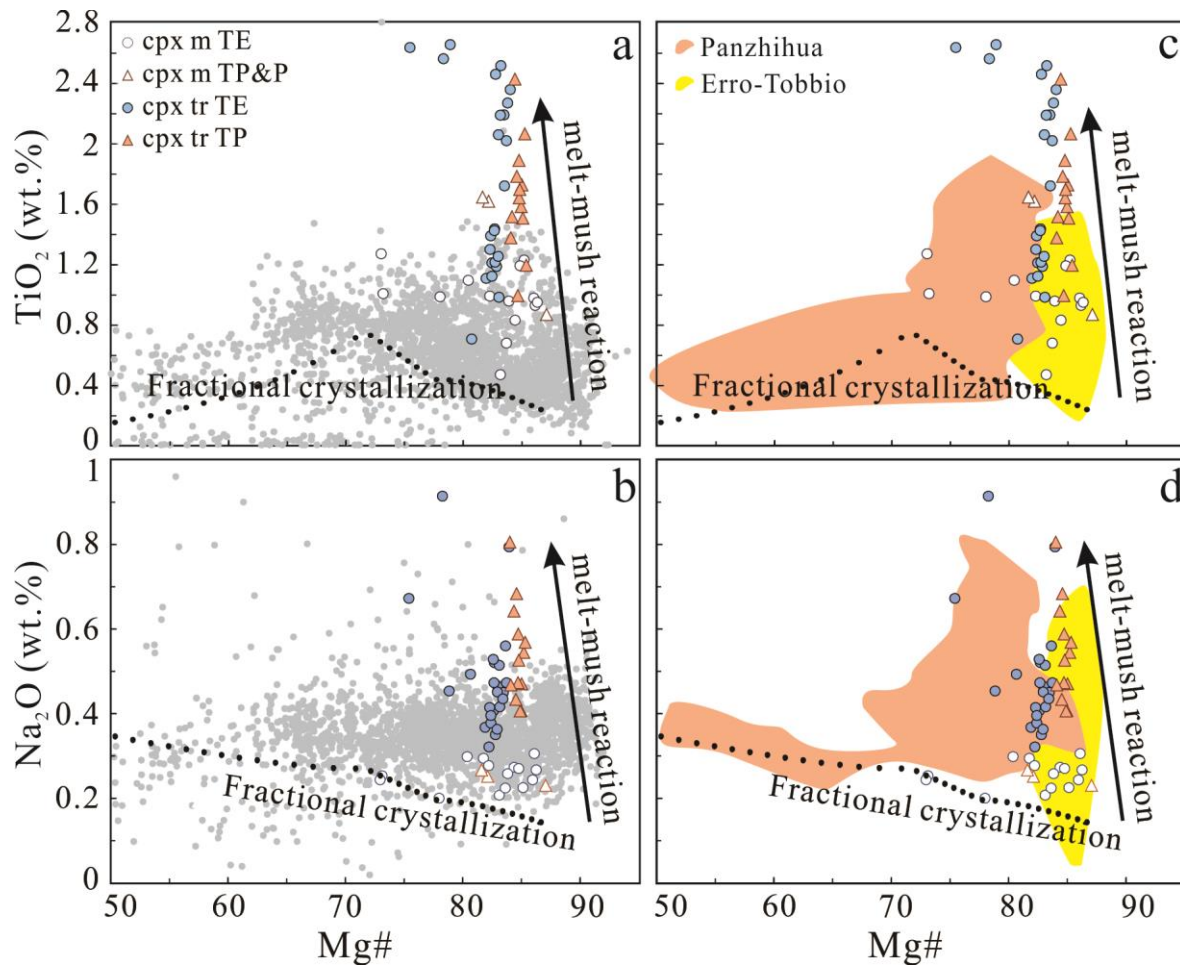
978
979



981
982

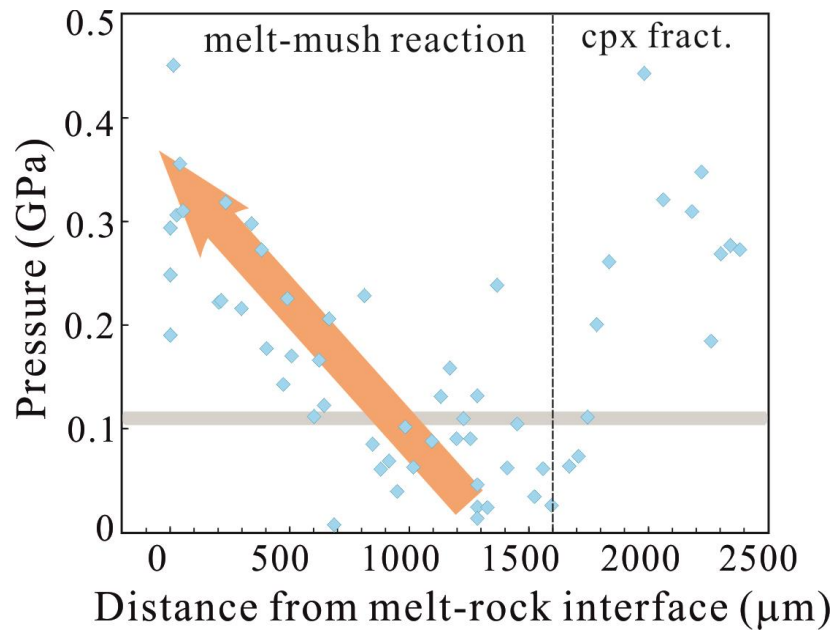


986



987

988



989

990

Table 1. Starting compositions (in wt.%)

Oxide	Primitive MORB ^a	Evolved MORB ^b	Plagioclase	Olivine
SiO ₂	50.13	50.49	47.57	41.54
TiO ₂	1.25	1.64	0.01	0.00
Al ₂ O ₃	16.31	14.29	32.88	0.03
Cr ₂ O ₃				0.01
FeO ^T	8.85	11.05	0.56	9.60
NiO				0.37
MnO	0.17	0.3	0.01	0.07
MgO	8.72	7.22	0.03	47.97
CaO	12.5	11.66	17.52	0.07
Na ₂ O	2.63	2.66	1.40	
K ₂ O	0.02	0.12	0.00	
P ₂ O ₅	0.08	0.18		
Total	100.66	99.61	99.98	99.65
Mg [#] /An/Fo	63.7	53.8	87.3	89.9

^a Major element composition of MORB sample KN182-13 D44A from Dr. Alberto Saal^b Major element composition of MORB MOA9812-095 from Dr. John Sinton^c All Fe as ferrous Fe to calculate Mg[#]**Table 2.** Summary of experimental conditions

	TE1	TE2/Es	TE_FC	TE_SC	TE_Ls	TE_mush ^a	TP1	TP2/Ps
Melt	Evolved					Evolved&Primitive	Primitive	
Pressure (kbar)	5	5	5	5	5	5	5	5
Initial temp (°C)	1180 (6h) ^b	1180 (6h)	1180 (6h)	1180 (6h)	1180 (27h)	1200 (6h)	1200 (6h)	1200 (6h)
Final temp (°C)	1180	1000	1000	1000	1000	1200	1200	1050
Cooling process	Quench	Step ^c	1°C/min	0.1°C/min	Step	Quench	Quench	Step
Total duration	6	26	9	35	48	6	6	26

^aTE_mush run used evolved melt to react with a troctolitic mush with 10% interstitial primitive melt^bNumber in parenthesis is the run duration at the specific temperature^cStep-cooling is at an average rate of ~ 0.15°C/min to the final temperatures